RSC Advances

REVIEW

View Article Online
View Journal | View Issue

Cite this: *RSC Adv.*, 2021, **11**, 3241

Recent advances in nanosized metal organic frameworks for drug delivery and tumor therapy

Junlei Yang,[a] Hui Wang,[a] Jinyao Liu,[a] Mengkui Ding,[a] Xianjin Xie,[a] Xiaoyu Yang,[a] Yaru Peng,[a] Shuang Zhou,[b] Ruizhuo Ouyang *[a] and Yuqing Miao[a]

Received 21st November 2020
Accepted 5th January 2021

DOI: 10.1039/d0ra09878g

rsc.li/rsc-advances

Metal organic-frameworks (MOFs) are novel materials that have attracted increasing attention for applications in a wide range of research, owing to their unique advantages including their small particle size, porous framework structure and high specific surface area. Because of their adjustable size, nanoscale MOFs (nano-MOFs) can be prepared as carriers of biotherapy drugs, thus enabling biotherapeutic applications. Nano-MOFs' metal ion catalytic activity and organic group functional characteristics can be exploited in biological treatments. Furthermore, the applications of nano-MOFs can be broadened by hybridization with other materials to form composites. This review focuses on the preparation and recent advances in nano-MOFs as drug carriers, therapeutic materials and functionalized materials in drug delivery and tumor therapy based on the single/multiple stimulus response of drug release to achieve the targeted therapy, offering a comprehensive reference for drug carrier design. At the end, the current challenges and prospects are discussed to provide significant insight into the design and applications of nano-MOFs in drug delivery and tumor therapy.

1. Introduction

Metal organic-frameworks (MOFs) arise from a self-assembly reaction involving metal ions or metal clusters with a special functional group of an organic chain, such as a carboxyl group or a nitrogen-containing heterocycle, enabling formation of complexes with a periodic network structure. Because of their myriad organic chains and metal clusters, MOFs are highly diverse. The high variability of the organic chain allows for the pore sizes of MOFs to be adjusted to meet different requirements. The adjustable material size and flexible skeleton structure of MOFs have attracted extensive attention in recent years, thus leading to in-depth research and applications of MOFs in sensing,[1] adsorption,[2] storage,[3] catalysis[4] and medical treatment.[5]

Tumors have been a major public health problem. Many people die of tumors each year, thus prompting extensive anti-tumor research in clinical treatments such as surgery, chemotherapy and radiotherapy (RT).[6] Although these treatments can attenuate tumor growth and metastasis to a certain extent, they exert little effect on most malignant tumors yet cause extensive damage to normal human organs in chemotherapy. This

[a]*Institute of Bismuth Science, University of Shanghai for Science and Technology, Shanghai 200093, China. E-mail: ouyangrz@usst.edu.cn*

[b]*Cancer Institute, Tongji University School of Medicine, Shanghai 200092, China*

Junlei Yang received his BS degree from Huainan Normal University, Huainan, China and is currently working toward an MS in chemical engineering within Dr Ruizhuo Ouyang's group at the University of Shanghai for Science and Technology. His research focuses are in the application of bismuth-containing nanomaterials in tumor diagnosis and treatment.

Hui Wang received her BS degree from Henan University of Science and Technology, China and is currently working toward an MS in biomedical engineering within Dr Ruizhuo Ouyang's group at the University of Shanghai for Science and Technology. Her research focuses on the application of nanomaterials in tumor therapy.

damage occurs because tumor growth differs from that of normal somatic cells, and anti-cancer drugs, after entering the systemic circulation, kill cells indiscriminately because of a lack of targeting. Therefore, materials have been explored as carriers to deliver drugs directly to tumor areas in targeted drug therapy, by taking advantage of the differences between normal somatic cells and the tumor microenvironment. The availability of nanomaterials such as liposomes[7] and micelles[8] has made drug loading possible. Nanoscale-MOFs (nano-MOFs) have been developed for drug-loading therapy, owing to their high specific surface area, adjustable pore size and good biocompatibility.[9] In addition, because nano-MOFs can be hybridized with other materials to form composites, their biomedical applications have been innovatively expanded to treatments including photothermal therapy (PTT),[10] photodynamic therapy (PDT)[11] and imaging-guided therapy.[12,13]

The nano-MOFs were used to be mostly applied for a single purpose like drug loading,[9] imaging,[12] *etc.* Here, the recent research progress of nano-MOFs in drug delivery combined with anti-cancer treatments are reviewed where the roles of nano-MOFs in cancer treatment as drug carriers, therapeutic materials and synergistic therapeutic materials are discussed to show their advantages in anti-cancer applications and potential future applications.

2. Preparation of nano-MOFs

Nano-MOFs are composed of different combinations of metal clusters and organic ligands. The pore size, shape and particle size of nano-MOFs are mostly related to the structure of organic ligands. In the process of preparing nano-MOFs such as solvothermal and hydrothermal synthesises, the formation of a regular framework material between metal ions and organic ligands requires external energy supply, like high temperature and high pressure. In addition, the way to change the energy supply form also enriches the preparation methods of nano-MOFs including sonochemical, microwave-assisted, mechanochemical, electrochemical synthesis.

2.1 Solvothermal and hydrothermal synthesises

Both solvothermal and hydrothermal synthesises are relatively traditional synthesis methods of MOFs. Usually, the metal salt and the organic ligand are added together to the organic solvent or water, and then transferred to the polytetrafluoroethylene reactor inside a stainless steel reactor for a certain temperature and time reaction. The nucleation and growth rate of nano-MOFs crystals can be controlled by changing the ratio of metal ions and organic ligands, solvent types, system temperature, pH value, reaction time, *etc.* under high temperature and pressure without

Jinyao Liu received his BS degree from Binzhou University, Shandong, China and is currently working toward an MS in chemical engineering within Dr Ruizhuo Ouyang's group at the University of Shanghai for Science and Technology. His research focuses on bismuth-based electrochemical immunosensor.

Mengkui Ding received his BS degree from Huainan Normal University, Huainan, China in 2014 and is currently working toward an MS in chemical engineering within Dr Ruizhuo Ouyang's group. His research interests are the fabrication of nanosized electrochemical immunosensors.

Xianjin Xie received his BS degree from Hefei Normal University, Hefei, China and is currently working toward an MS in chemical engineering within Dr Ruizhuo Ouyang's group. His research focuses on the application of electrochemical sensors in microRNA detection.

Xiaoyu Yang is currently working toward an MS in applied chemistry within Dr Ruizhuo Ouyang's group at the University of Shanghai for Science and Technology. His research interest is the preparation and applications of bismuth-based electrochemical immunosensors.

changing the structure of the organic ligand. Either solvothermal or hydrothermal method for nano-MOFs preparation is not only simple and stable but also can control the size and properties of the crystals, and therefore is suitable for the synthesis of most nano-MOFs. For example, the porous MIL-53 [14] and UiO-66 [15] were easily synthesized using solvothermal method.

2.2 Sonochemical synthesis

As for the sonochemical method, ultrasonic waves are typically used to perform strong ultrasonic treatment on the liquid by adjusting the frequency of the sound wave so that the ions in the reaction liquid can obtain high energy, promoting the progress of the chemical reaction. In this process, by controlling the sound wave frequency, the reaction time can be greatly shortened and the uniformity of the formed product can be improved as well. In addition, this method is conducive to improving yield, operating safety, and reducing reaction costs. For example, using ultrasound-assisted methods, HKUST-1,[16] MOF-5,[17] and MIL-88A (Fe)[18] were successfully synthesized with uniform crystal structures.

2.3 Microwave-assisted synthesis

Microwave refers to electromagnetic waves with a wavelength range from 0.1 mm to 1000 mm and the corresponding frequency window of 300 MHz to 3000 GHz. Microwave synthesis is widely applied in the chemical synthesis due to its strong penetration, high efficiency, rapid response, safety and non-toxicity. Polar solvents such as water, alcohols, and *N*,*N*-dimethylformamide are mostly used to synthesize nano-MOFs. These polar solvents can be quickly and uniformly heated by microwave in the solution, which greatly shortens the reaction time and is safe to operate compared to traditional solvothermal and hydrothermal methods. For example, some nano-MOFs such as MOF-74 [19] and MIL-140 [20] were produced as predicted using microwave synthesis.

2.4 Mechanochemical synthesis

Mechanochemistry refers to the chemical reaction under the action of mechanical external force like shear, extrusion, friction, impact. Mostly, the reaction occurs between solid phases.

Yaru Peng is currently working toward an MS in applied chemistry within Dr Ruizhuo Ouyang's group at the University of Shanghai for Science and Technology. Her research interest is the preparation and applications of bismuth-based electrochemical immunosensors.

Shuang Zhou received his Ph.D. degree in tumor immunology from Fudan University, China in 2009. He is currently working as associate professor at Tongji University School of Medicine. His research interests are in the basic and translational medicine study of tumor biotherapy.

Ruizhuo Ouyang received her PhD degree in Analytical Chemistry from Nanjing University, Nanjing, China under the supervision of Prof. Huangxian Ju in 2008. Afterwards, she went to The University of Tennessee, Knoxville, TN, USA for 3 years as a postdoctoral researcher. Currently, she is an associate professor at the University of Shanghai for Science and Technology. Her research mainly focuses on the exploration and preparation of novel bismuth-based nanomaterials including nanosized metal hybrids, molecularly imprinted polymers, metal organic frameworks, etc., *their applications in bioassays, bioelectrocatalysis, biosensing and nano-electrochemistry.*

Yuqing Miao is a full professor of chemistry at the University of Shanghai for Science and Technology, China. He gained his MS degree from Nanyang Technology University, Singapore, and his PhD degree from Wuhan University of Technology, China. His research interests are in electroanalysis and biosensors. Current research concerns self-adsorption and nanostructures of ultrathin metal ions (especially Bi and Ni) with a size below nanoscale; interfaces synthesis and assembly of transition metal hydroxide enanostructures, their electrocatalytical and analytical applications for biothiols, organophosphorus toxicants, glucose and formaldehyde. The research also combines biomimetics and nanotechnology to develop test strips or dip sticks, reagent kits and electrochemical biosensors.

Compared with the traditional synthesis methods, mechanochemical synthesis is simple and easy to operate without using high temperature and high pressure, and suitable for mass production. Since the reaction does not produce a large amount of waste liquid, mechanochemical synthesis is considered as an environmentally friendly method, and attractively selected to prepare some nano-MOFs, such as the synthesis of MOF-74 analogues[21] and Ni-MOF.[22]

2.5 Electrochemical synthesis

In the process of electrochemical synthesis, a chemical reaction occurs through the gain and loss of electrons on cathode and anode to provide energy for the redox reaction. To synthesize nano-MOFs, the electrodes are placed at both ends in solution containing metal salt, organic ligand and solvent followed by optimizing the parameters such as solvent electrolyte, voltage, current and others. This method is free of high temperature and high pressure, and thus greatly shortens the reaction time, where electron transmission, a clean energy source, supplies the reaction energy. More importantly, the production of by-products can be effectively avoided through controlling current and voltage, increasing the yield. The electrochemical synthesis has been applied to produce nano-MOFs such as DMOF-1-Zn[23] and Cu-MOF.[24]

3. Nano-MOFs as drug carriers

The drug carriers are characteristic of good biological description, high loading rate and controllable release. According to the particle size, the drug carriers usually present as microspheres (1–250 μm) and nanoparticles (NPs) (1–1000 nm) for different application purposes. However, as tumor drug carriers, the following requirements must be met first: (1) good biocompatibility; (2) high loading rate of drugs; (3) controllable drug release in the organism; (4) being catabolized and metabolized.

During the transfer of drug molecules into tumor cells by nanoparticles, the carrier is first transported around the tumor cells *via* the blood circulation, and then internalized by tumor cells. The uptake of nanomaterials by cells is mainly through endocytosis, which includes phagocytosis and pinocytosis. Phagocytosis is mainly caused by the uptake of large particles, while pinocytosis mainly uptakes smaller particles. The internalization process of nanomaterials is affected by both the mediating proteins (cavourin and clathrin) on the cell surface and the shape, size, charge as well as surface modification of nanomaterials. It has been confirmed that the shape affects mainly the aspect ratio of nanomaterials. For example, the cell internalization was the most when the particle size of the studied nanomaterial is about 50 nm obtained by adjusting the aspect ratio of the material. As generally believed, cell membranes are negatively charged and have a higher uptake rate of positively charged nanomaterials. Therefore, the uptake of carrier by cells can be increased through positively modifying the materials. For surface modification of nanomaterials, as some specific proteins are overexpressed on the outer surface of tumor cells, the outer surfaces of the nanocarriers can be modified with targeting material which can specially recognize specific proteins on tumor cells to increase the uptake rate of the carrier material.

Research on nano-MOFs has made rapid progress in recent years, and these materials' high specific surface area and adjustable pore size have prompted extensive exploration of applications. Antineoplastic drugs are primarily hydrophobic agents, thus resulting in difficulties in drug entry into the circulation and absorption *in vivo*. Consequently, a protective material to encapsulate or adsorb anti-cancer drugs is necessary to increase their therapeutic effects. A variety of drug carriers, such as liposomes,[25] nanoemulsions,[26] hydrogels,[27] micelles[28] and nanoparticles[29] have been developed and found to greatly enhance drug absorption. However, these drug carriers have the drawbacks of low drug loading rates, ineffective release, poor blood circulation and negligible biological toxicity. Nano-MOFs with high specific surface area are advantageous, owing to their adjustable pore sizes and good biocompatibility, and therefore may be ideal drug carriers. To improve the therapeutic effects on tumors, targeted carriers have been developed through the design of nano-MOFs that degrade and release drugs in specific tumor microenvironments, thereby achieving targeted therapy.[30] The existing mechanisms of targeted drug release based on nano-MOFs are classified as pH response, ion response, temperature response, pressure response and redox response. Moreover, owing to the easy functionalization of nano-MOFs, the targeted release of drugs can be achieved by modifying biofilms or macromolecules outside nano-MOFs.[31]

3.1 pH response

The microenvironments of tumor cells, in contrast to normal cells, results in altered oxygen uptake in tumor cells, owing to the abnormal growth of tumor tissues. Most tumor cells use anaerobic respiration to produce more acid, and therefore, the microenvironment of tumor cells is more acidic than that of normal cells. pH responsive degradation of nano-MOFs can be achieved by adjusting the organic chains inside nano-MOFs. ZIF-8 has been successfully used as a carrier to load the anti-cancer drug doxorubicin (DOX) and prepare DOX@ZIF-8.[32] ZIF-8 has been synthesized under alkaline conditions by using 2-methylimidazole as an organic ligand, which undergoes a protonation reaction with H^+ in acidic environments, thus causing the collapse of ZIF-8 and the entrapment or adsorption on the material, and ultimately pH-responsive drug release. In addition, nano-MOFs have been modified by materials with a protonation and deprotonation pH responsive mechanism, thus achieving pH responsive drug release. Chitosan (CS), which has good biocompatibility, has been used to externally modify nano-MOFs.[33] The surface modification of nano-MOFs with CS improves the biocompatibility of nano-MOFs, and the amino groups of CS can also be protonated at low pH, thus forming abundant hydrogen bonds and leading to drug release. However, at a higher pH, skeleton shrinkage of the material occurs, owing to the deprotonation reaction. This mechanism can enable smooth drug release at low pH and has great potential in drug delivery.

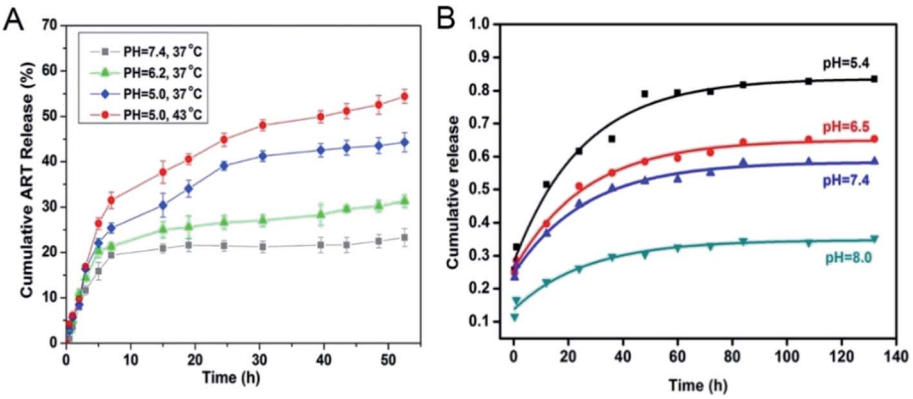

Fig. 1 (A) *In vitro* release profiles of ART-loaded-MOFs under different pH values (pH 7.4, pH 6.2 and pH 5.0) and temperatures (37 °C and 43 °C).[34] This figure has been reproduced from ref. 34 with permission from Elsevier, copyright 2016. (B) DS released from MIL-125 in PBS at pH 8.0, 7.4, 6.5 and 5.4 from 0 to 132 h.[35] This figure has been reproduced from ref. 35 with permission from Elsevier, copyright 2018.

Environmental changes often affect the structures of nano-MOFs. Therefore, nano-MOFs that are unstable under acidic conditions can be used as carriers to transport drugs. Nano-MOFs containing Fe(III) carboxylic groups are pH sensitive and can be used as drug carriers. MIL-100 (Fe) has been synthesized for loading artemisinin (ART). As shown in Fig. 1A,[34] with MIL-100 (Fe) at the same temperature, the ART release is pH responsive, increasing significantly at low pH; the skeleton of MIL-100 (Fe) collapses, and ART is released at lower pH. Additionally, MIL-125 with an octahedral structure has been found to remain intact at pH 8.0 after immersion of MIL-125 (Ti) in phosphate buffered solution (PBS) solutions at different pH for 1 week; however, the material disappears in solutions at pH 5.4 and 4.0,[35] thus suggesting that MIL-125 (Ti) is pH sensitive and can be applied for loading diclofenac sodium (DS). Fig. 1B shows that the release of DS gradually increases from 35% (pH 8.0) to 80% (pH 5.0) within 132 hours, thus indicating the ability of MIL-125 to release the drug at low pH. Moreover, other Fe-based nano-MOFs, such as MIL-53,[14,36] MIL-100-NH_2 [37] and MIL-101 [38] have been applied in pH responsive drug transport.

For the different types of nano-MOFs mentioned above, ZIF-8 or MOF modified with CS is used as a carrier. The acid response is mainly due to the protonation of organic ligands or modified groups with H^+ in an acidic environment, causing slow decomposition of MOF structure in an acidic environment. Therefore, the drug exhibits a high pH-dependent release as the pH decreases at low pH (5.0–6.0) till achieving the complete release of the drug. While at high pH (6.5–8.0), the decrease of H^+ in the environment leads to a gradually decreasing drug release with the increase of pH due to the decrease in the protonation of the carrier structure. For example, the structure of MIL-*M* (*M* = 100/53/101) dissociates in a slightly acidic environment.[14,37,38] The increasing acidity of the environment accelerates the dissociation of its structure and release of drug molecules. The loading of drug molecules into nano-MOFs drugs mainly relies on physical adsorption and chemical bonding. Drug molecules such as DOX, ibuprofen (Ibu), *etc.* enter into the nano-MOFs pore size through electrostatic interaction or free diffusion and shows high pH-dependent release. However, the drug loading through forming weak chemical bonds is relatively stable. A high release rate of drug molecules is usually achieved after the carrier structure is destroyed.

3.2 Ion response

Because of the diversity of the physiological environment in the body, the abundant ions in the tissue fluid can participate in drug release from nano-MOFs. MOF-74-Fe^{3+}, a low toxicity cation, has been prepared for drug delivery: MOF-74-Fe^{2+} was first synthesized and oxidized to MOF-74-Fe^{3+} for Ibu loading, and 15.9 wt% loading was achieved.[39] The mechanism of drug release has been described to occur in two stages. As shown in Fig. 2A, in the early stage, Ibu negative ions release drugs through ion exchange or free diffusion. Later, Fe^{3+} preferentially coordinates PO_4^{3+}, thereby achieving anion-triggered drug release.

An anionic bio-MOF-1 has been synthesized through introduction of an organic ligand into adenine;[40] dimethylammonium cations in the skeleton pore of bio-MOF-1 are then ion-exchanged with exogenous cations. The application of procainamide has been explored in biological drug delivery. As shown in Fig. 2B, under the physiological conditions of PBS rich in Na^+ cations, the loaded procainamide cation interacts with Na^+ in organisms and releases drug molecules. Fig. 2C shows that the release of procainamide in deionized water is stable in the first 20 hours and is completed by 72 hours. In comparison, drug release from bio-MOF-1 in PBS is significantly better, thus indirectly demonstrating the ion-responsive drug release of bio-MOF-1.

A Zr-based MOF (UiO-66-NH_2) has been constructed as a drug carrier through modification with carboxylatopillar[5]arene (CP5),[41] which acts as a supramolecular switch enabling ion-triggered release of cargo molecules through competition with exogenous Zn^{2+} to link MOFs (Fig. 2D). Drug therapy for neurological diseases is not ideal; however, the synaptic vesicles in the nervous system are rich in zinc, thus making UiO-66-NH_2 favorable for loading neurotherapeutic drugs to overcome these

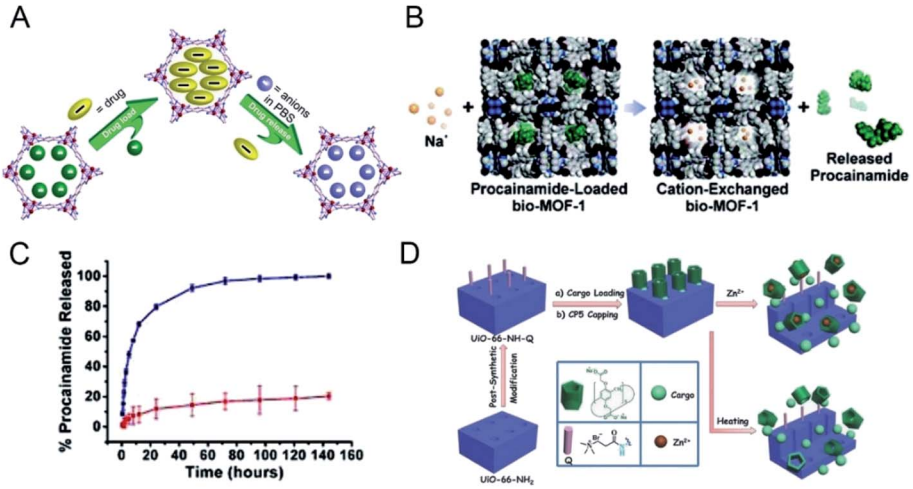

Fig. 2 (A) Schematic diagram of drug loading and release process.[39] This figure has been reproduced from ref. 39 with permission from American Chemical Society, copyright 2014. (B) Scheme depicting cation-triggered procainamide release from bio-MOF-1; (C) procainamide release profiles from bio-MOF-1 (blue, PBS buffer; red, deionized nanopure water).[40] This figure has been reproduced from ref. 40 with permission from American Chemical Society, copyright 2009. (D) Schematic representation of stimuli-responsive mechanized UiO-66-NH_2 MOFs equipped with positive charged quaternary ammonium salt (Q) encircled by pillarene[2]pseudorotaxanes.[41] This figure has been reproduced from ref. 41 with permission from Wiley-VCH Verlag & Co. KGaA, copyright 2015.

limitations. UiO-66-NH_2 can achieve targeted drug release of different amounts of drug molecules according to the concentration of Zn^{2+} in synaptic vesicles in the patient's nervous system, thus decreasing the adverse effects of drugs and exerting better therapeutic effects. In addition, drug release through an ion response can be triggered by integration of DNA nucleic acid chains into nano-MOFs.[42,43]

3.3 Redox response

The complexity of the organic chain allows diversification of the types of nano-MOFs. The differences between the tumor microenvironment and the normal cell environment can be exploited for drug release. According to previous studies,[44] tumor cells have higher levels of glutathione (GSH) than normal cells. Because GSH has reducing properties, nano-MOFs can be synthesized by using oxygen-reducing materials. First, the disulfide bond is easily reduced and introduced into the organic chains of nano-MOFs for drug-loading treatment of tumors, and the abundant GSH in the tumor cells enables redox responsive drug release with fewer adverse effects and enhanced therapeutic effects.[45] For example, a Mn-MOF synthesized by using dithiol dihydroxyacetic acid as an organic ligand and Mn^{2+} as metal center, has been used for drug delivery after being modified with dopamine and polyethylene glycol (PEG).[46] Because the organic ligand contains a disulfide bond, the excess GSH in the tumors reduces the disulfide bond, thus resulting in the backbone collapse of nano-MOFs and subsequent drug release. Similarly, with 4,4′-dithiobisbenzoic acid (4,4′-DTBA) as an organic ligand, MOF-M (DTBA) (M = Fe, Al, Zr) has been synthesized by selecting a variety of metals.[47] Fig. 3 shows the control of the morphology and size of the MOFs by using different synthesis temperatures. Small dimensions of nanomaterials for biological applications can increase the *in vivo* circulation cycle of the material. MOF-Zr (DTBA) of approximate 125 nm has been produced by using Zr as the metal center at a synthesis temperature of 40 °C. The loading and encapsulation efficiency values of the drug curcumin (CCM) are 11.8% and 78.7%, respectively. DTBA enters cancer cells through an enhanced permeability and retention effect. Similarly, the abundant GSH in tumor cells reduces the disulfide bond inside DTBA, thereby resulting in skeleton collapse of DTBA and the release of curcumin. Redox-responsive drug release has been achieved with an inhibition rate of 76.1%.

In addition, new properties can be conferred on nano-MOFs by loading biological macromolecule enzymes. For instance, glucose enzyme (GOx)/insulin have been encapsulated into ZIF-8 to form insulin-GOx/ZIF-8 (Ins-GOx/ZIF-8).[48] Here, glucose enters the pores of Ins-GOx/ZIF-8 after entering the body and is oxidized to gluconic acid and H_2O_2 while contacting the GOx, thus causing a pH decrease around the Ins-GOx/ZIF-8. Because ZIF-8 itself exhibits pH responsive degradation, a low pH directly leads to the drug release and subsequent therapeutic effects. Ins-GOx/ZIF-8 could be used for anti-tumor therapies, in which the acidic tumor microenvironment enables the pH responsive degradation of ZIF-8. Moreover, additional application prospects arise from the consumption of glucose inside the tumor, thus further weakening the tumor energy supply and killing tumor cells.

3.4 Other responses

The structural complexity and easy functionalization of nano-MOFs allow for diverse application mechanisms, including single stimulus response and multi-stimulus responses, beyond the abovementioned release methods. Temperature changes often affect the structural integrity of nano-MOFs, and release of the cargo molecules can be controlled by temperature changes around the nano-MOFs during application. Two Zn-based MOFs, ZJU-64 and ZJU-64-CH_3, have been formed from the

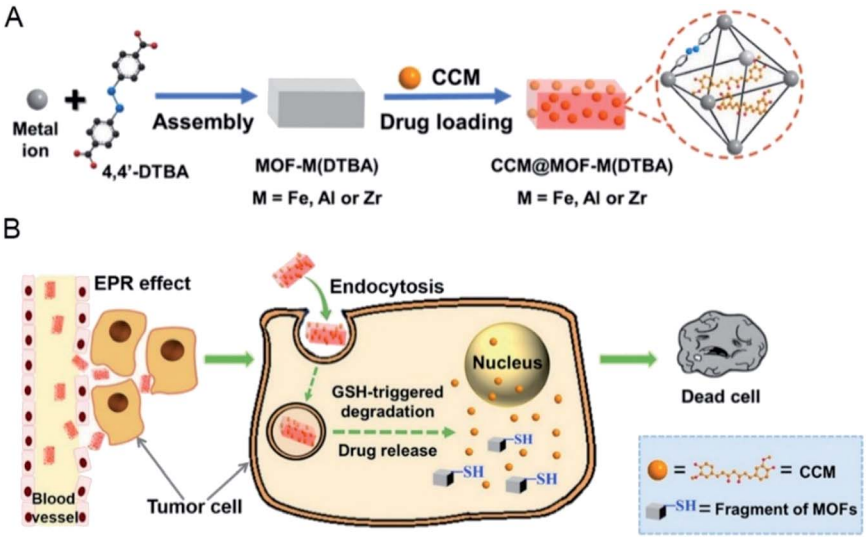

Fig. 3 Schematic illustration of (A) the preparation of CCM@MOF-M(DTBA), and (B) the redox-responsive degradation of CCM@MOF-M(DTBA) in tumor cells for cancer therapy.[47] This figure has been adapted from ref. 47 with permission from American Chemical Society, copyright 2018.

non-toxic metal ion Zn^{2+} thus resulting in secondary building structures with the biological macromolecule adenine.[49] These MOFs have been loaded with the anti-cancer drug methotrexate (MTX) in two forms: one in which the inner layers of MTX and ZJU-64 and ZJU-64-CH_3 are relatively stable through hydrogen bonding and π–π connection, and the other in which the outer layers of MTX are interconnected, and the main connection is a weak π–π interaction. During the release phase, the drug is rapidly released during the first 4 hours and is then slowly released. The MTX release significantly increases from 37 °C to 60 °C at the same pH (Fig. 4A), thus indicating that the interactions among ZJU-64, ZJU-64-CH_3 and the drug molecule are interrupted when the temperature is raised, thereby releasing MTX. Zn-TBDA (TBDA = 4′-(1*H*-tetrazol-5-yl)-[1,10-biphenyl]-3,5-dicarboxylic acid) has also been used to load MTX;[50] similarly, increased temperature attenuates or interrupts the interaction between the host and cargo molecules, thus releasing the drug molecule MTX.

New functions can be imparted to nano-MOFs by taking advantage of their unique physical and chemical properties. Through incorporating magnetic materials into MOFs for drug-loading based anti-tumor therapy, magnetic responsive drug release can be achieved. Fe-based magnetic materials are often used to encapsulate or adsorb onto nano-MOFs for functionalization. For example, $Cu_3(BTC)_2$ (H_2BTC = 1,3,5-benzenetricarboxylic acid) has been used to coat magnetic Fe_3O_4 to achieve long-acting drug release by adsorption of the anti-tumor drug nimesulide into pores of the MOFs (Fig. 4B).[51] After encapsulation of drugs in MOFs, the magnetic properties are not substantially affected, thus indicating the magnetic targeting ability of the composite. γ-Fe_2O_3@ZIF-8 and γ-Fe_2O_3@MIL-53(Al) have successfully been formed by encapsulating superparamagnetic γ-Fe_2O_3 into ZIF-8 and MIL-53(Al);[52] the final product retains high magnetic properties and can achieve phased drug release (Fig. 4C). The magnetic properties of MOFs can also be used for magnetic targeting of drugs. S. Sharma has used magnetic MOF MIL-88B to load drugs and found that the products exhibit good magnetic targeting capabilities.[53] To achieve targeted drug delivery to tumor cells, specific targeting groups are mostly modified on the surface of carrier materials used in the traditional targeted therapy. However, under an external magnetic field, the magnetic MOFs carrier can accurately reach the tumor site due to the strong magnetic response without causing damage to the organism. More importantly, the magnetic screening can be performed after drug loading to improve the targeting ability. Moreover, by changing the direction and frequency of the applied magnetic field, the drug release can be controlled,[54] showing great potential for the application of targeted tumor therapy. On the other hand, the magnetic materials can be used for magnetic resonance imaging (MRI) diagnosis and treatment due to the magnetic resonance.

In drug loading and release, the drug carrier can be specially treated to prevent the drug from being released and thus to prolong the release time by overcoming the initial burst-like release of the drug molecule. In this regard, some temperature or pressure treatments may be applied to force a physical change in the structure of the carriers after drug loading to control the drug release. A Zr cluster-based nano-MOFs ZJU-800 has been synthesized for DS loading and subjected to different pressures of 0 MPa, 10 MPa and 30 MPa.[55] The release time of the drug extends from 2 days to 8 days as the applied pressure increases (Fig. 4D). Under different pressures, the pore collapse of the ZJU-800 skeleton occurs to different degrees, thereby preventing the rapid release of the drug and prolonging the drug release time. Similarly, two MOFs, NU-901 and NU 1000, have been used as carriers to load drugs[56] and a sustained drug release effect has been achieved, owing to the partial collapse of the MOF skeleton. For the temperature-sensitive MOF carriers, the increase in temperature tends to destroy the structural

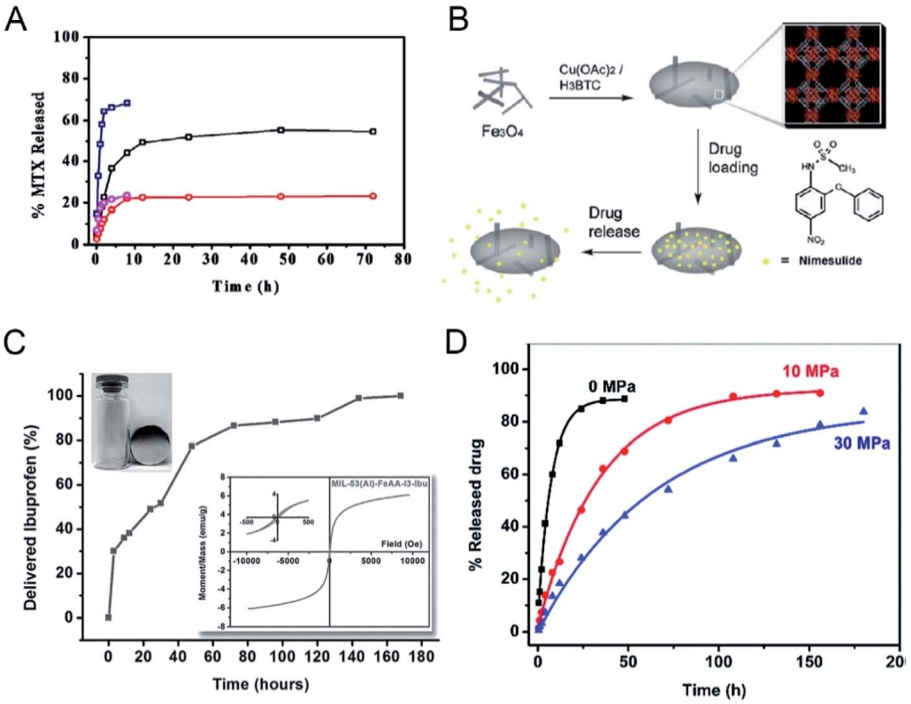

Fig. 4 (A) MTX release profiles of MTX-loaded ZJU-64 and ZJU-64-CH_3 at different temperatures under intestinal conditions (pH 7.4). Black, MTX-loaded ZJU-64 at 37 °C; red, MTX-loaded ZJU-64-CH_3 at 37 °C; navy, MTX-loaded ZJU-64 at 60 °C; magenta, MTX-loaded ZJU-64-CH_3 at 60 °C.[49] This figure has been reproduced from ref. 49 with permission from Wiley-VCH Verlag & Co. KGaA, copyright 2016. (B) An illustration of the synthesis and action of $Fe_3O_4/Cu_3(BTC)_2$ nanocomposites for potential targeted drug release.[51] This figure has been reproduced from ref. 51 with permission from Royal Society of Chemistry, copyright 2011. (C) Ibuprofen delivery from MIL-53(Al)-FeAA-I_3. Inset: the separation of the sample under the external magnetic field and corresponding magnetization curves.[53] This figure has been reproduced from ref. 53 with permission from Wiley-VCH Verlag & Co. KGaA, copyright 2014. (D) DS release from ZJU-800 with a pressure of 0 MPa (black), 10 MPa (red), and 30 MPa (blue). The curves were fitted using non-linear regression.[55] This figure has been reproduced from ref. 55 with permission from Royal Society of Chemistry, copyright 2011.

integrity of the carrier. The drug molecules are released from the entire nano-MOFs through destroying the coordination bond between the metal clusters and the organic ligands. The temperature increase weakens the interaction between the drug molecule and the nano-MOF carrier, leading to the release of drug molecules, called thermal release. Moreover, the thermo-sensitive nano-MOFs can be combined with photothermal reagents for trial use to improve the effect of photothermal treatment and increase the release of drugs in the tumor.

Since some biomolecules such as genes and proteins can stimulate the structure change of nucleic acids, nucleic acids can be coated outer of MOF carriers and open their structure in a specific environment to release drug molecules. As known, tumor cells grow faster than normal cells. Under sufficient energy supply, tumor cells will produce more glycolysis and therefore produce more adenosine triphosphate (ATP) than normal cells, providing a new research direction for the design of responsive drug delivery materials. W. Morris[57] conjugated to the surface of NMOF-N_3 (Fig. 5) with a nucleic acid probe functionalized with dibenzocyclooctyne (DBCO), and explored its colloidal stability and cell transfection ability. Based on this work, W. Chen[58] and his colleagues synthesized a MOF material with similar structure (Fig. 6A). The drug molecules or fluorescent molecules were loaded in the pores with the nucleic acid locked on the surface of the MOF material by hybridizing the nucleic acid strands. In the presence of the over-expressed ATP in tumor cells, the ATP aptamer bound to the intracellular APT to release the drug. A good response release effect was achieved, as shown in Fig. 6B, wherein X represented the anti-ATP aptamer sequence, and Y the aptamer sequence containing ATP-AS1411, which can specifically recognize the tumor nucleotide receptor unit. It can be seen from Fig. 6C and D that, in the presence of ATP, the release of fluorescent dyes and drug molecules was much greater than that without ATP. Afterwards, polyacrylamide was cross-linked on the outer surface to achieve the construction of a multi-stimulus response carrier.[59]

In addition, taking advantage of the sensitivity of nucleic acid to external stimuli, J. Kahn[43] synthesized a DNA-functionalized nano-MOFs (Fig. 7A), which could release drugs based on the response to multiple stimuli of pH and K^+ by changing the type of nucleic acid in the outer layer (Fig. 7B and C).

There are many types of polymers with different properties. After modifying the MOF materials with polymers, the properties of the nano-MOFs like biocompatibility may be improved to broaden the application range of nano-MOFs. Y. Zhang[60] and his colleagues used UiO-66 as a carrier to support the photosensitizer iridium compound, which was modified with a dual-

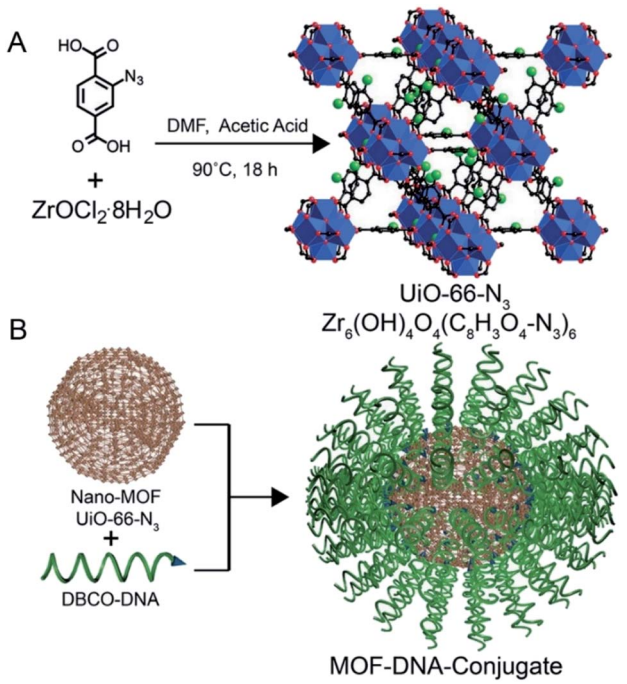

Fig. 5 (A) Synthesis of UiO-66-N_3 ($Zr_6O_4OH_4(C_8H_3O_4{-}N_3)_6$) nanoparticles. (B) DNA functionalization of UiO-66-N_3 nanoparticles, utilizing DNA functionalized with dibenzylcyclooctyne (DBCO). Blue: zirconium atoms; red: oxygen atoms; black: carbon atoms; green: azide groups. Hydrogen atoms are omitted for clarity.[57] This figure has been adapted from ref. 57 with permission from American Chemical Society, copyright 2014.

response ionic polymer, poly[(2-acryloyl)ethyl-(*p*-boronic acid pinacol ester benzyl)-diethylammonium bromide] (BP) on the outer surface, and poly[2-(5,5-dimethyl-1,3-dioxan-2-yloxy)ethyl acrylate] (PDM) and cyclodextrin-functional poly(glycerol methacrylate) (PG), abbreviated as BP-PDM-PG. In the presence of reactive oxygen species (ROS), BP could reverse the charge through its multi-cation section and weaken the electrostatic interaction with the MOF material to release the loaded material. PDM showed also a certain pH response performance. When the physiological pH changed to acidic conditions, PDM changed from hydrophobicity to hydrophilicity, which was beneficial to the release of loaded materials. As shown in Fig. 8A, when the pH value dropped from 7.4 to 5.4, the release of iridium compounds increased from 2.26% to 35.1% within 3 days. Compared with the uncoated polymer, when the light produced more ROS, the release amount of iridium compounds increases from 32.6% to 73.2% at pH 5.4, demonstrating excellent response release ability. Here, poly(*N*-isopropylacrylamide) (PNIPAM) was heat-sensitive and poly(acrylic acid) (PAA) pH-sensitive. PNIPAM dissolves in water at temperature below 32 °C and accumulates above this temperature. S. Nagata[61] and his colleagues wrapped the copolymer of PNIPAM and PAA on the surface of MOF carrier to endow the MOF with ability to respond to pH and heat. As shown in Fig. 8B, the changes in pH and temperature could switch drug release of the prepared MOF material.

For some responsive materials, polymer packaging can reduce the external environment's stimulation of the materials so as to protect the internal material and slowly degrade the material. Y. Liu[62] modified Zr-MOF with azobisisobutyronitrile (AIBN) and polymer (such as poly(*N*,*N*′-bis(acryloyl)cystamine) (PAC), poly(acrylic acid) (PAA)) to improve the overall stability of Zr-MOF as it is unstable in a phosphate environment and prone to degradation. In addition, the destruction of disulfide bonds inside PAC in tumor cells under GSH-rich conditions was the cleavage of the Zr-MOF structure to achieve the redox response to drug release.

The controllable transport of light-driven drug carriers is widely used in the therapy. Light can be divided into ultraviolet (UV, 200–200 nm), visible light (400–750 nm) and near infrared (750–2000 nm) according to different wavelengths. There are differences in properties of different wavelengths, such as UV rays, which have high energy and strong biodegradation, but poor penetration, suitable for use on the surface of objects. On the contrary, near-infrared (NIR) light has strong penetrating ability, low background signal, relatively weak energy, and weak biological toxicity, so the light control response carrier mostly refers to the drug release of NIR light touch. Using a light-responsive MOF as carrier material, the photosensitive characteristics of the material should be first considered. Under UV light, azidobenzene can undergo photoisomerization and act as a photosensitive material. For example, J. Brown[63] synthesized an azidophenyl containing MOF, which could release the loaded dye molecules under UV irradiation. However, the stability of the MOF in aqueous solution was still an obstacle, hindering its application. X. Meng[64] and his colleagues synthesized Zr-MOF (UiO-68-azo) containing an azide group with β-cyclodextrin (β-CD) modified outside, where rhodamine-B (RhB) was used instead of drugs for adsorption. The modification of β-CD made UiO-68-azo produce competitive release and controllable drug release under UV conditions. Under UV irradiation, the azidobenzene was isomerized, accordingly the β-CD ring was separated from the stem, releasing the drug molecule. With the UV lamp off, the drug release showed a significant decrease.

Z. Luo[65] synthesized the photosensitive MOF material PCN-244 which was coated with a copolymer of di-(1-hydroxylundecyl)selenide (DH-Se), biocompatible PEG, and poly(propylene glycol) (PPG), a randomly polymerized coating poly(DH-Se/PEG/PPG urethane) to serve as a carrier for drug loading. It was found that under the irradiation of a visible light (λ = 488 nm), the obtained photosensitive material generated active oxygen, which triggered the cleavage of the outer layer of the copolymer carrier, leading to the drug release (Fig. 9A). As can be seen from Fig. 9B, by comparison, the release amount of drug molecules was significantly increased after the visible light was applied, achieving the light-responsive drug release. In the NIR range, organic ligands such as porphyrins are commonly used as photosensitizers to participate in the synthesis of nano-MOFs. This type of materials can react with O_2 to produce active oxygen and be used for photodynamic therapy owing to the good absorption in the NIR region.

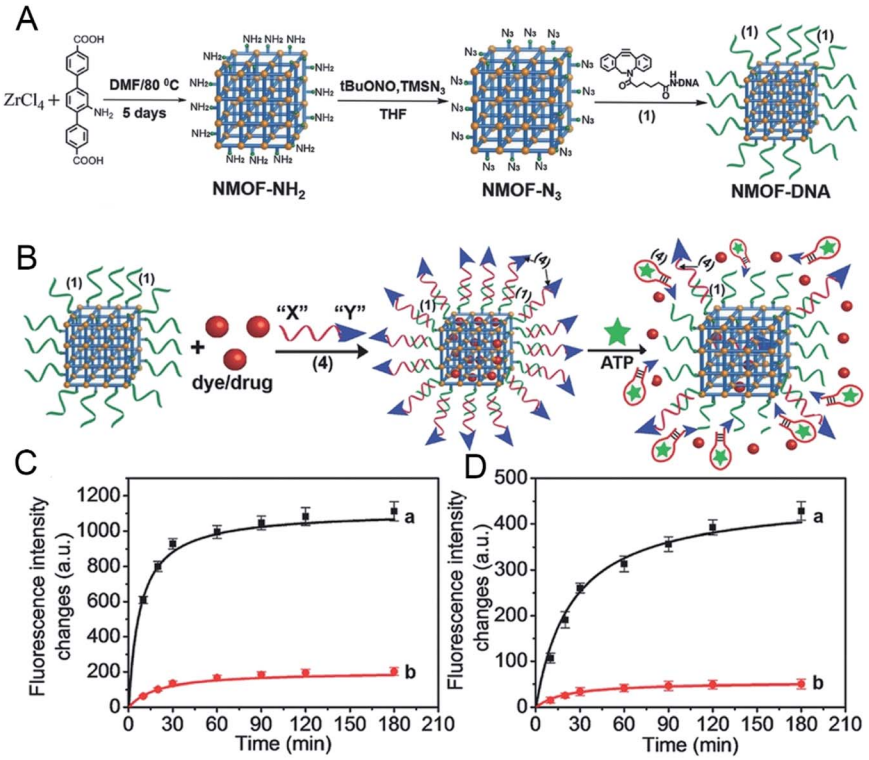

Fig. 6 (A) Synthesis of the nucleic acid (1)-functionalized NMOFs. (B) Locking of the rhodamine 6G or DOX in the (1)-modified NMOFs by the formation of the (1)/(4) duplex lock, where (4) includes the anti-ATP aptamer sequence "X" and the AS1411 sequence "Y". The resulting NMOFs include the AS1411 as targeting sequence and the ATP aptamer sequence as unlocking mechanism in the presence of ATP being overexpressed in cancer cells. (C) The time-dependent release of rhodamine 6G from the loaded NMOFs: (a) in the presence of ATP, 25×10^{-3} m; (b) in the absence of ATP. (D) The time-dependent release of doxorubicin from the loaded NMOFs: (a) in the presence of ATP, 25×10^{-3} m; (b) in the absence of ATP. (Error bars derived from $n = 3$ experiments.).[58] This figure has been reproduced from ref. 58 with permission from Wiley-VCH Verlag & Co. KGaA, copyright 2017.

Although a single response release mechanism can target tumor tissue, the therapeutic effects relative to those with a multi-stimulation response release mechanism are unclear. In recent years, composite materials have been widely used through combining other materials with nano-MOFs, thus endowing MOFs with new functions. Fe_3O_4 has been introduced into UiO-66-NH_2 (Zr) by using water-soluble carboxylatopillar[6]arene (WP6) as a nanovalve to endow UiO-66 with pH and ion responsive release,[66] and 1-(6-bromohexyl)pyridinium bromide (Py) has been used as a linker between Fe_3O_4@UiO-66-NH_2 and WP6. The interaction between the WP6 ring and Py stalk decreases with increasing temperature, thereby resulting in the release of drug molecules. This structure has excellent application prospects and could be used in chemotherapeutics combined with PTT. Moreover, several other response mechanisms can be combined to achieve multi-stimulus response release.[67,68]

Diverse drug release mechanisms have endowed nano-MOFs with different functions. Currently, nano-MOFs are increasingly used for target drug delivery by combining the nano-MOFs with other materials to form complexes that exhibit multi-stimulus responses to drug release and significantly improved drug targeting ability. Compared to traditional carrier materials such as liposomes, polymer nanoparticles, mesoporous silica, and inorganic nanomaterials, nano-MOF materials as drug carriers have higher carrying efficiency due to their unique skeleton structure. Compared with inorganic nanomaterials, nano-MOFs show better biocompatibility and less biological toxicity and can be catabolized more easily by organisms. Due to the diversity and easy functional modification of nano-MOFs, the responsive nano-MOFs carriers can be designed to achieve responsive release of cargo molecules, especially biological macromolecules without destroying their biological activity. To understand the applications of these responses more comprehensively, we summarize the recent stimulus responses of nano-MOFs in drug delivery in Table 1.

As shown in Table 1, the release mechanism of the pH-responsive nano-MOFs is divided into protonation effect and pH cleavable bond. The protonation effect usually changes the environment structure by changing the pH of the environment, part of which is reversible, while the pH cleavable bond refers to an irreversible chemical bond break in an acidic environment. For ion response, the structures of the nano-MOFs are interfered with the abundant ions in the organism, leading to the release of the drug because of ion exchange. With regard to both the redox response and the enzyme response, the drug molecules are similarly released as structure of the nano-MOFs are opened as a result of the chemical reaction between redox

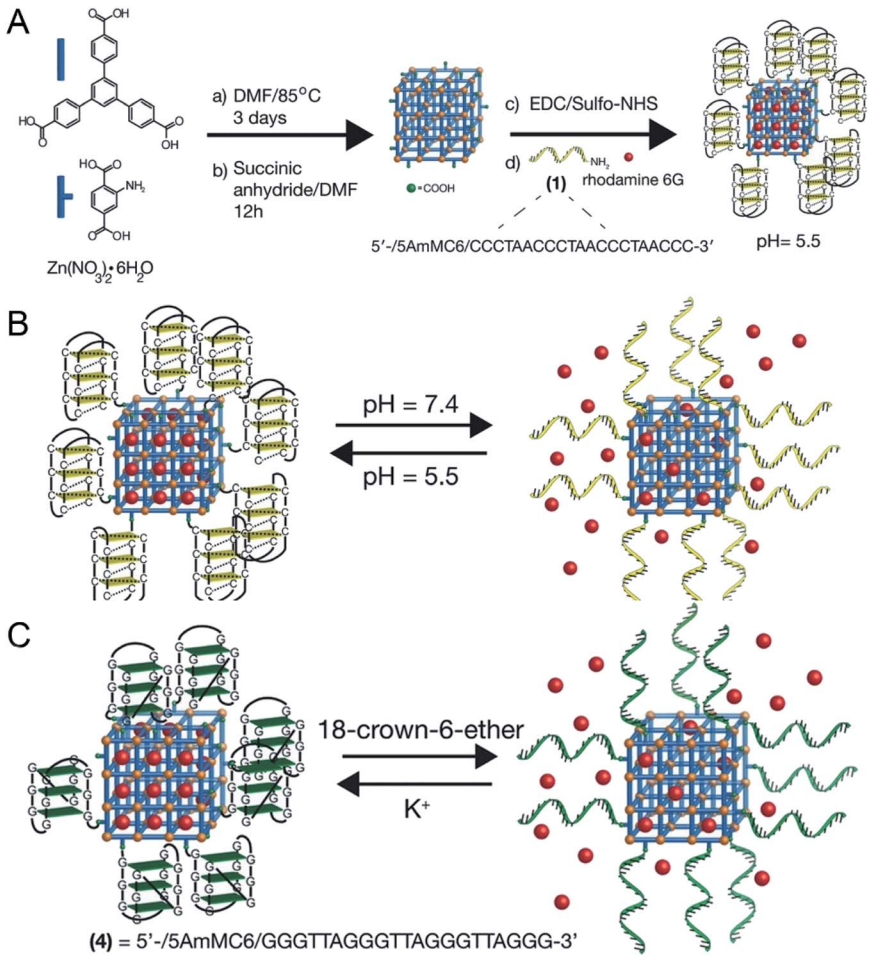

Fig. 7 (A) Synthesis scheme for the preparation of the i-motif-gated rhodamine 6G-loaded MOFs. (B) Scheme of pH-stimulated switchable release of the rhodamine 6G-loaded MOFs gated by i-motif units. (C) Scheme of the switchable cyclic ON–OFF release of the rhodamine 6G load from K^+-stabilized G-quadruplex-gated MOFs. The release is initiated by the presence of 18-crown-6-ether.[43] This figure has been reproduced from ref. 43 with permission from Wiley-VCH Verlag & Co. KGaA, copyright 2016.

agents and enzyme molecules more abundant in tumor cells than normal cells. The thermal response is based on either the thermal expansion of the nano-MOFs or the thermal cracking of the structure due to the change of the external temperature. Under a magnetic field, the magnetic nano-MOFs can target the drug into the tumor sites and increase the release of the drug inside the tumor to achieve the effective therapeutic effect, which is called the magnetic response.

In addition to loading tumor drugs, nano-MOFs can be used to delivery other therapeutic drugs. Traditional insulin is usually administered by injection due to the low efficiency of oral administration. The structure of the acid-resistant MOF NU-1000 is complete in the gastric acid environment and degraded in the physiological environment, so MOF NU-1000 was selected to load insulin[89] for therapeutic purpose, where the absorption rate of insulin for oral administration was greatly improved, showing a good application prospect. ZIF-8 could wrap on the surface of the virus vaccine without damaging its structure, and thus protect vaccine from being broken during its storage and transportation.[90] Also, nano-MOFs shows good antibacterial potential.[91]

4. Nano-MOFs as therapeutic materials

The porosity and high specific surface area of nano-MOFs have been extensively exploited in drug delivery. However, the organic chains forming nano-MOFs vary, and some organic chains with characteristic functions can be selected to coordinate with specific metals without altering their specific properties. Nano-MOFs with new functions have consequently been produced, thus enriching the application field of MOFs, particularly in tumor treatment.

4.1 Rational utilization of metal ions

On the basis of the difference between the microenvironments of tumors *versus* normal tissues, nano-MOFs can be designed to target tumors. Fenton reaction means that in a mixed solution containing H_2O_2 and Fe^{2+}, Fe^{2+} can catalyze H_2O_2 to produce O_2 and hydroxyl radical. The hydroxyl radical has strong oxidative damage ability due to the oxidation potential of 2.8 V. Nano-MOFs show excellent catalytic activity because of the transition metals of active sites. For example, Fe^{2+} exhibits good

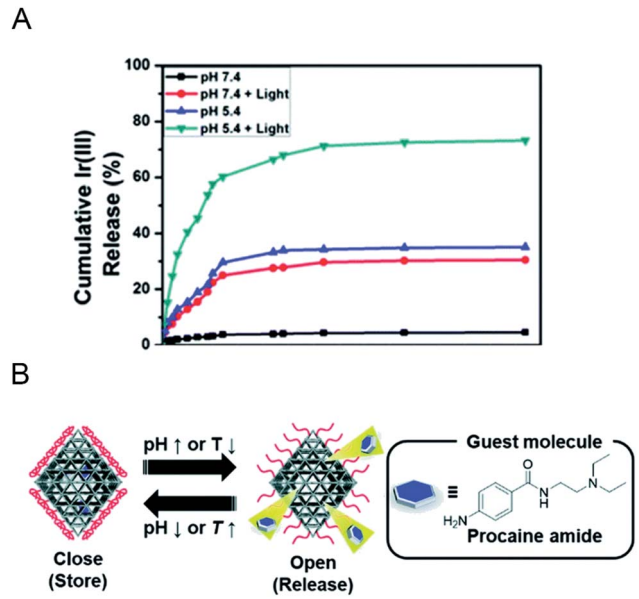

Fig. 8 (A) Cumulative release profile of the Ir(III) complex from Ir@MOF/BP-PDM-PG NPs under different conditions.[60] This figure has been reproduced from ref. 60 with permission from Royal Society of Chemistry, copyright 2020. (B) Schematic image for preparing MOFs controlled release using UiO-66-P(NIPAM-AA).[61] This figure has been reproduced from ref. 61 with permission from Royal Society of Chemistry, copyright 2020.

catalytic properties in acidic environments, and the Fenton reaction can result in the production of oxygen and active free radicals by H_2O_2, which in turn promotes tumor cell apoptosis. Fig. 10 shows the synthesis of MOF-Fe^{2+}, followed by the successive loading of dichloroacetic acid and liposomes.[92] The optimum pH value for the Fenton reaction of Fe^{2+} is between 2.0 and 5.0, and the pH of the tumor microenvironment tends to be higher. However, the release of the loaded dichloroacetic acid decreases the pH of the microenvironment to approximately 4.0, thus resulting in the best catalytic effect of Fe^{2+}. Consequently, MOF-Fe^{2+} catalyzes the production of more active free radicals by H_2O_2, thereby promoting apoptosis and killing tumors. Furthermore, an MOF with an oxidizing metal element has been used to produce an oxidizing active substance to treat tumors. X. Gao *et al.* have found that MIL-125 synthesized with Ti^{4+} produces superoxide free radicals under ultraviolet irradiation,[93] thereby confirming the relatively low toxicity of MIL-125 and the clear killing effect in HePG-2 cells under ultraviolet irradiation (Fig. 11). Z. He[94] synthesized Zr-based porphyrin MOF with Au nanoparticles connected on the outer surface as radiosensitizers. The Au nanoparticles endowed the Zr-based porphyrin MOF with catalase-like activity of catalyzing H_2O_2 to produce O_2 and enhance the effect of radiotherapy and chemotherapy for O_2-dependent tumors. In addition, based the principle that Cu can catalyze the azide–alkyne cycloaddition reaction, F. Wang[95] modified Cu on the surface of Zr-MOF to synthesize resveratrol analogues *in situ* within the mitochondria, where obvious therapeutic effects were received as expected.

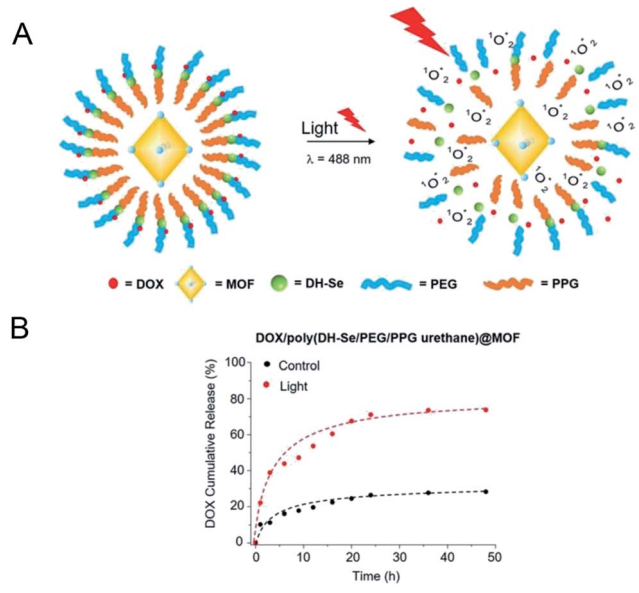

Fig. 9 (A) Graphical illustration of *in vitro* drug release from DOX/poly(DH-Se/PEG/PPG urethane) @ MOF nanocomposite upon light radiation. (B) The accumulative release behavior of DOX *in vitro* from DOX/poly(DH-Se/PEG/PPG urethane)@MOF nanocomposites with or without light.[65] This figure has been adapted from ref. 65 with permission from Wiley-VCH Verlag & Co. KGaA, copyright 2019.

4.2 Rational use of organic ligands

PDT is a tumor treatment method that uses lasers and photosensitizers, where lasers with specific wavelengths excite the photosensitizer to react with surrounding O_2, generating singlet oxygen. Singlet oxygen can oxidatively damage tumor cells and promote their apoptosis. Porphyrin derivatives are preferred photosensitizers that can produce ROS under irradiation with specific light sources in tumor cells. The use of synthetic nano-MOFs with porphyrin derivatives can impart new functions. Various types of MOFs contain porphyrin derivatives and rely on the porphyrin derivatives' photosensitizing properties. Fe-carboline derivatives act as photosensitizers for PDT in tumors. Fe-TPB (TPB = 5,10,15,20-tetra(*p*-benzoato)porphyrin) has been synthesized by using the TPB as the organic chain,[96] with the size controlled to approximately 100 nm. Because of the Fenton reaction caused by iron ions under the abundant H_2O_2 in tumors, more O_2 is produced, thus alleviating the hypoxic environment of tumor cells. The production of ROS in PDT is decreased in a hypoxic environment within tumors, thereby diminishing the therapeutic effects. The Fenton reaction increases O_2 production and directly increases the effects of downstream PDT treatment. In the tumor environment, MOFs containing porphyrin derivatives combine with O_2 and form ROS after being irradiated by a specific light source, then oxidatively bind biological macromolecules, damage the cells and cause cell death (Fig. 12). In addition, the porous coordination network (PCN) series (Zr-MOF) are widely used MOFs in PDT.[97,98] For example, the synthetic PCN-224 has been applied to PDT treatment.[99] To overcome the high GSH

Table 1 Examples of stimulation response of MOF materials

Stimuli	MOFs	Mechanism	Carrier	Loading percentage [wt%]	Ref.
pH	ZIF-8	Protonation effect	DOX	20.0	32
	ZIF-8		Gelonin	40.0	69
	ZIF-8		Imiquimod, 1-methyl-D-tryptophan	8.9, 10.7	70
	Zn-MOF		5-Fluorouracil (5-Fu)	34.3	71
	CS/Bio-MOF-13-Co		DOX	48.1	33
	IRMOF-3		DOX	61.5	72
	MIL-125 (Ti)	pH-cleavable bonds	Diclofenac sodium	13.6	35
	MIL-101-NH_2		Camptothecin	18.0	37
	MIL-100 (Fe)		Metformin hydrochloride	35.0	73
	Fe-MOF		DOX	42.9	74
	Zn-MOF		5-Fu	44.6	75
	MIL-53 (Fe)		Oridonin	56.3	36
Ions	UiO-66-NH_2	Ion exchange	5-Fu	1.5	41
	MOF-74-Fe^{3+}		Ibuprofen	15.9	39
	MOF-In		5-Fu	34.3	76
	Bio-MOF-1		Procainamide	18.0	40
Redox	Mn-MOF	Reduce the disulfide bonds	DOX	50.0	46
	MOF-Zr (DTBA)		Curcumine	11.8	47
	CD-MOFs		DOX	4.3	45
	Fe-MOF		DOX	6.4	77
Temperature	ZJU-64/ZJU-64-CH_3	Thermal-responsive materials	Methotrexate	13.5/10.6	49
	ZJU-801		Diclofenac sodium	41.7	78
	Zn-MOF	Thermal expansion	—	—	79
Magnetic	HKUST-1	Magnetic-responsive materials	Nimesulide	16.7	51
	γ-Fe_2O_3@MIL-53(Al)		Ibuprofen	9.9	52
	Fe-MOF		DOX/methylene blue	0.7/4.3	53
Enzyme	Fe-MOF	Enzyme-response material	DOX	1.9	80
	UiO-68		Camptothecin	2.5	81
Pressure	ZJU-800	Pressure-responsive materials	Diclofenac sodium	58.8	55
NIR	Pd-MOF	NIR-cleavable bonds	Hydrogen	—	82
pH, ions	Zn-MOF	Acid degradation and electrostatic interaction	Ibuprofen	—	83
	Zn-MOF		Rhodamine 6G	—	43
	ZIF-8		DOX	9.1	84
pH, NIR	MIL-100 (Fe)	pH, NIR-cleavable bonds	DOX	12.8	85
	ZIF-8		DOX	26.4	86
	MIL-53 (Fe)		DOX	90.0	14
pH, redox	ZIF-8	pH, redox-cleavable bonds	DOX	19.1	87
	ZIF-8		GOx/insulin	1.5/4.9	88
	Fe-BTC		DOX	28.6	68
pH, ions, thermo	Zr-MOF	pH, ions, thermo-cleavable bonds	5-Fu	3.1	67
	UiO-66		5-Fu	9.7	66

content in tumors and neutralize the generated ROS, MnO_2 has been modified on the surface of PCN-224 to improve the therapeutic effects, given that Mn^{4+} can undergo a redox reaction with GSH. On the one hand, the intracellular GSH content can be reduced in this process. On the other hand, Mn^{4+} can be reduced to Mn^{2+} with magnetic resonance imaging ability, thereby guiding the PDT process. Similarly, Mn-MOF has been synthesized through a one-pot method from porphyrin derivatives and Mn^{3+}, which is reduced to Mn^{2+}, thereby resulting in magnetic resonance imaging ability in the presence of the abundant GSH in cells.[100] The fluorescence imaging function of porphyrin and the characteristics of sensitizer have been examined and found to show very good application prospects in PDT.

4.3 Comprehensive utilization of materials

Carbon-based nanomaterials have good photothermal conversion efficiency (PCE) and can be used in cancer treatment.[101] However, carbon-based nano-MOFs have relatively fewer applications in photothermal conversion. P. Yang *et al.* have synthesized ZIF-8 as a basic material by adjusting the ratio of raw materials.[102] The desired carbon nanoparticles (ZCNs) have been synthesized and modified with PEG for applications in biological therapy. The ZCNs show good photothermal and photoacoustic imaging effects. More importantly, as the sizes of nanoparticles increase, the photothermal effect increases (Fig. 13). On the basis of the quantum yield of ROS produced by indocyanine green (ICG), when the sizes of ZCNs increase, the quantum yield of ZCNs exceeds that of ICG, thus leading to

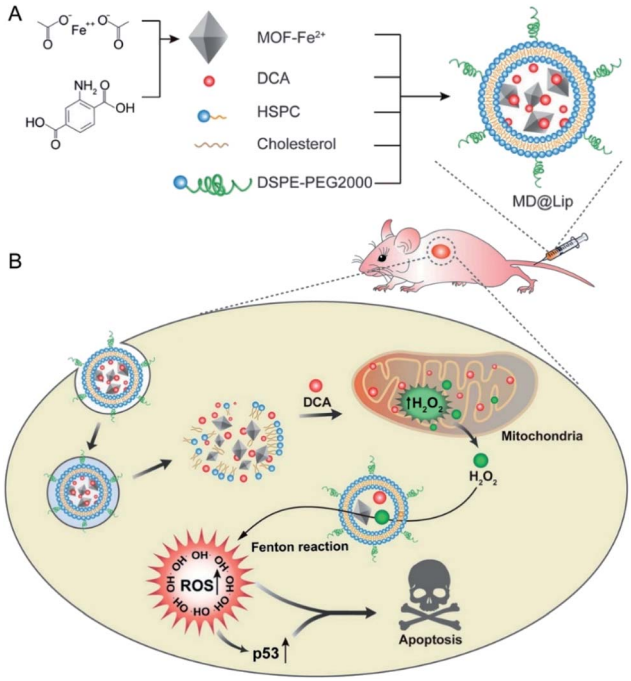

Fig. 10 Liposome-based combination therapy of dichloroacetic acid (DCA) and MOF-Fe^{2+} (MD@Lip) for enhancing antitumor effects. (A) Preparation of MD@Lip nanoparticles. (B) MD@Lip-induced apoptosis in cancer cells. MD@Lip can not only stimulate H_2O_2 generation in mitochondria, but also improve the Fenton reaction to produce $^{\bullet}OH$, consequently inducing cellular apoptosis.[92] This figure has been adapted from ref. 92 with permission from Wiley-VCH Verlag & Co. KGaA, copyright 2019.

good therapeutic effects. ZIF-8 has also been used as the base material to form a core–shell structure material with SiO_2 coating.[103] After pyrolysis, SiO_2 is removed, thereby forming carbon nanostructures and endowing the nano-MOFs with a porphyrin like metal center. The carbon-based nano-MOFs are a good sound sensitive agent that can be used in acoustic therapy.

Microwave hyperthermia is a new method using a microwave sensitizer to treat tumors and kill tumor cells through heating under microwave radiation; this method is safe and reliable, and greatly diminishes harm.[104–106] Because of their high specific surface area, good biodegradability and diverse structure, nano-MOFs can be used as a microwave sensitizer in microwave hyperthermia. Small-sized Mn–Zr MOF has been synthesized and found to effectively release loaded drugs after heating of the materials with microwave radiation. The microwave heat conversion efficiency of the Mn–Zr MOF has been found to reach 28.7%, and favorable effects of cooperative treatment have been reported.[107] A popcorn-shaped Zr-MOF has been synthesized with large cracks on the surface, thus overcoming the drawback of the poor ion trapping ability of MOFs. The material diameter has been controlled at 250 nm *via* to adjustment of the synthesis method, thus making the DOX loading more conducive to absorption of the material through the porous structure of Zr-MOF. The synthesis of Zr-MOF effectively improves the microwave heat conversion efficiency and provides good therapeutic effects (Fig. 14).[108]

Many explorations of organic ligands have indicated the therapeutic effects of nano-MOFs. Multifunctional organic chains do not show changes in their original properties that affect their applications and treatment effects after binding to metal ions (Table 2). In addition, organic ligands can be synergized with metals to achieve better therapeutic results. However, this basic design is generally combined with drug therapy, and the efficacy of monotherapy is often lower than that of synergistic therapy.

5. Nano-MOFs as synergistic therapeutic agents

In modern methods of treating tumors, many new functional materials have been developed, including some photosensitive particles such as CuS,[114] Bi_2S_3,[115] Au,[116] Bi_2Se_3,[117] carbon-based materials[118] and polymer nanoparticles.[119] These materials have been extensively used in the treatment of cancers. The framework structure of nano-MOFs is composed of metal clusters and organic ligands, which can be functionalized provide a great possibility for surface modification. During the

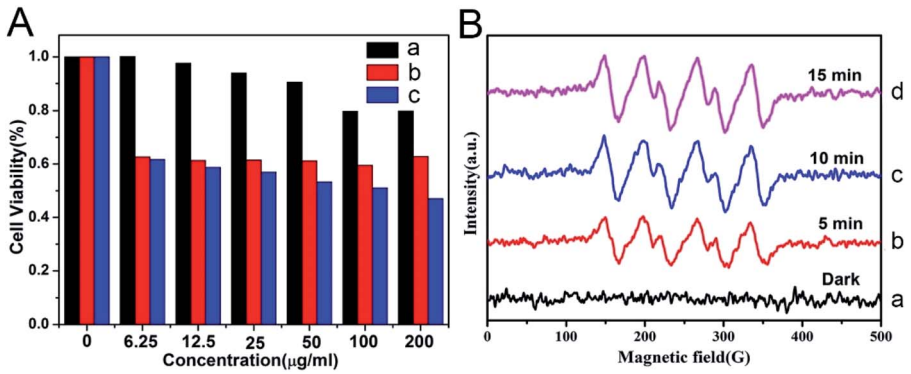

Fig. 11 (A) Viabilities of HepG-2 cancer cells after being cultured with Prussian blue (PB)@Ti-MIL-125 (a), after UV-irradiation for 30 min (b), after being cultured with PB@Ti-MIL-125 and UV-irradiation for 30 min (c). (B) Electron paramagnetic resonance (EPR) spectra of DMPO-$^{\bullet}O^{2-}$ adducts of PB@Ti-MIL-125 in darkness and under visible light irradiation with different irradiation times.[93] This figure has been reproduced from ref. 93 with permission from Elsevier, copyright 2019.

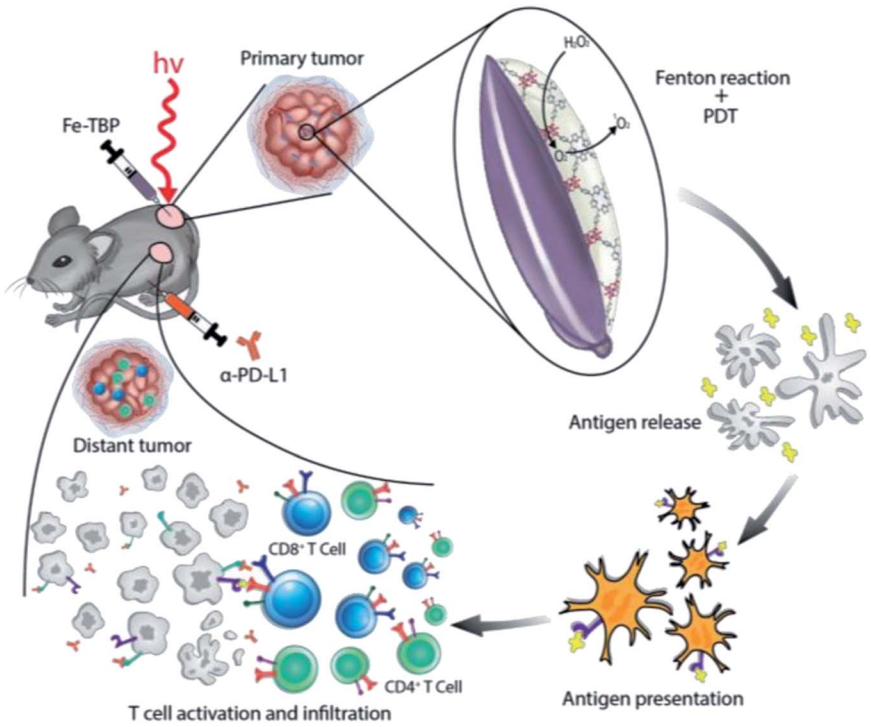

Fig. 12 Illustration of using Fe-TBP to overcome hypoxia for PDT primed cancer immunotherapy.[96] This figure has been adapted from ref. 96 with permission from American Chemical Society, copyright 2018.

synthesis of nano-MOFs, diverse functional groups on the organic chain such as carboxyl, amino, and hydroxyl can be introduced to the outer surface of the nano-MOFs favorable for later functional modification. Also, metal clusters with saturated coordination in the framework structure of nano-MOFs can form coordination with organics, providing convenience for post-synthesis modification. With the widespread use of nano-MOFs in drug delivery and treatment, researchers have combined photosensitive particles and nano-MOFs, endowing them with the properties of photosensitive materials. The application prospects of PTT and PDT in tumor treatment have been recognized. Combinations of nano-MOFs and other functional materials have been applied to PTT and PDT, thus extending the applications of nano-MOFs.

5.1 Nano-MOF modified photosensitizers for PTT

Polymeric molecules with photothermal properties can be used as PTT agents for tumor therapy, among which, polypyrrole (PPy), polydopamine and polyaniline are most commonly used. PPy is a good optical PTT reagent, owing to the π-conjugation effect, and it has been widely used in biological therapy because of its favorable biocompatibility.[120–122] Nano-MOFs can be modified with PPy in two ways. One is forming PPy by introducing the parent molecular polymer molecule inside nano-

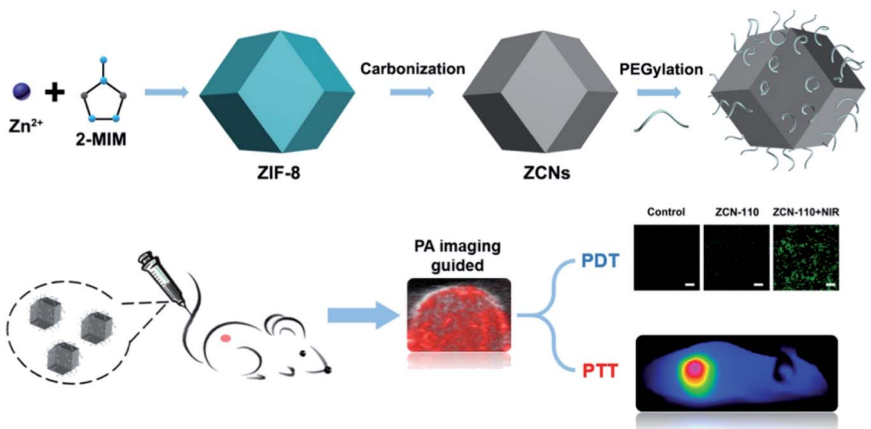

Fig. 13 Schematic diagram of preparing ZIF-8 derived carbon nanoparticles (ZCNs) and their applications in *in vivo* photoacoustic (PA) imaging guided photothermal/photodynamic combined therapy.[102] This figure has been adapted from ref. 102 with permission from American Chemical Society, copyright 2018.

MOFs to polymerize the pyrrole monomer on the surface, thus achieving PTT.[123] The other is converting the pyrrole monomer to PPy by combining the oxidizing nano-MOFs;[14] this method is more convenient to perform. Similarly, nano-MOF modified with polydopamine can also be used as photoacoustic contrast agents to achieve chemotherapy-PTT in combination with drugs, owing to their high biocompatibility and PCE.[124,125] Polymerization of aniline monomers (polyaniline) on the surfaces of nano-MOFs can be performed with an oxidizing agent to achieve a photothermal treatment effect similar to that of PPy, as shown in Fig. 15.[15]

Nanoparticles used for single PTT have achieved therapeutic effects in the treatment of tumors,[126] but the treatment effects are often lower than those of systems combined with other materials. Therefore, nanoparticles with photothermal properties have been encapsulated into materials such as nano-MOFs to impart photothermal conversion properties to nano-MOFs. PB is a dye reagent that exists as colloidal nanoparticles and is widely used in cancer treatment, owing to its favorable biocompatibility and high PCE.[127] By growing MOFs outside PB nanoparticles, drugs can be loaded for tumor PTT. D. Wang *et al.* have used MIL-100 (Fe) to encapsulate PB nanoparticles that form a core–shell structure,[34] which combines the photothermal properties of PB particles and the photoluminescence of MIL-100 (Fe) for magnetic resonance imaging (Fig. 16). The obtained composite shows low toxicity and good therapeutic effects. CuS, Bi_2S_3, Au, MoS_2 and other materials exhibit enhanced light absorption properties in NIR, where light energy penetrates the human body to the maximum extent; therefore, these materials are generally used for tumor PTT.[128] Synthesized CuS nanoparticles have been added into the framework of ZIF-8 for PTT.[129,130] Because of the pH-responsive degradation of single ZIF-8, the ZIF-8 skeleton is protonated and degraded, thus releasing CuS nanoparticles in the tumor microenvironment, which can be heated to kill cancer cells through NIR radiation. Similarly, Au,[131] Bi_2S_3 [132] and Bi_2Se_3 [133] have been combined with nano-MOFs to achieve photothermal effects.

In addition, carbon-based materials, such as graphene quantum dots, possess good absorption properties in the NIR region and a high light conversion rate; these materials have been encapsulated in nano-MOFs for PTT.[134]

5.2 Nano-MOF modified photosensitizers for PDT

Sensitizer as a kind of compound containing conjugated system can produce intermediates (free radicals) with higher activity through absorbing specific wavelength of laser energy and undergoing photochemical changes. These photosensitizers are advantageous of photosensitivity and high intermediate yield, and therefore can be used as carriers or therapeutic agents for disease treatment. For example, the photosensitizer is excited by laser without damaging the organism in the process of tumor treatment. Given the higher content of H_2O_2 in tumor cells than in normal cells, H_2O_2 or O_2 can be converted into singlet oxygen through a photosensitizer. The singlet oxygen combines with biological macromolecules in

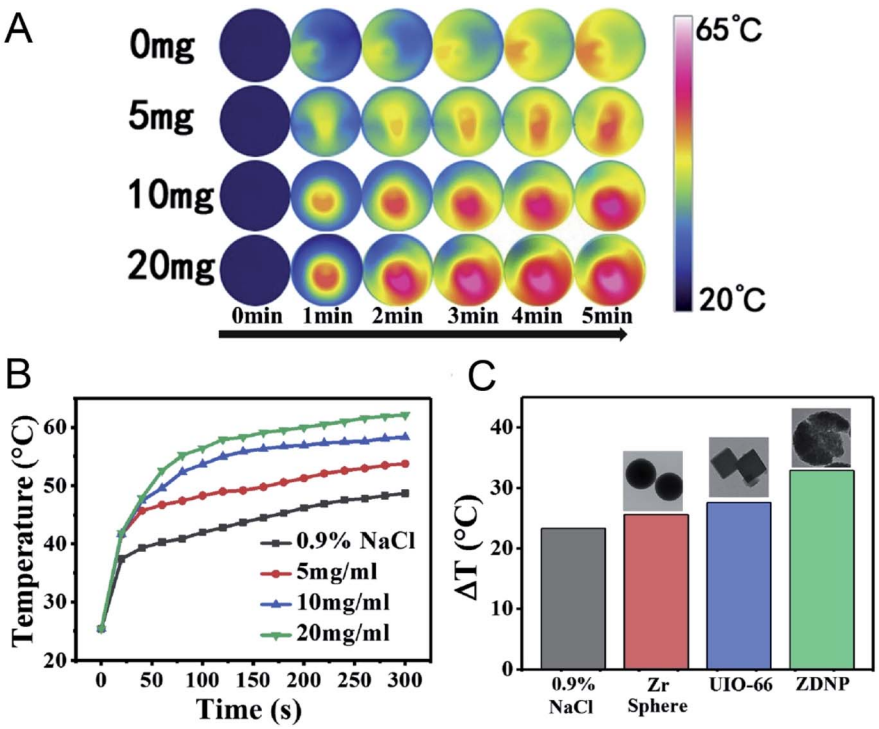

Fig. 14 (A) The infrared thermal images of Zr-MOFs at different concentrations irradiated by microwave. (B) The temperature record of MW irradiated Zr-MOF. (C) The comparisons of temperature rise among Zr-MOF, Zr-sphere and UIO-66.[108] This figure has been adapted from ref. 108 with permission from Elsevier, copyright 2020.

Table 2 Examples of nano-MOFs for tumor treatments

Functional components	Major components	MOFs	Mechanism	Treatment type	Ref.
Ions	Fe	Zr-Fc MOF	Fenton reaction	Chemodynamic therapy	109
	Fe	MIL-100	Fenton reaction	Chemodynamic therapy	110
Organic ligands	Porphyrinic	PCN-224	Photodynamic effect	PDT	97
	Porphyrinic	Hf-TCPP	Photodynamic effect	PDT	111
	Porphyrinic	Cu-MOF	Photodynamic effect	PDT	112
	Porphyrinic	Zr-FeP MOF	Photodynamic effect	PDT, photoacoustic imaging	113

cells and breaks the structure of DNA, thus resulting in apoptosis. These photosensitizers include methylene blue,[135] black phosphorus,[136] ICG[137] and cyanine dye.[138] These photosensitizers are integrated into nano-MOFs is the same manner as photosensitizers in PTT. During the encapsulation of photosensitizers into nano-MOFs, the photosensitizers are usually synthesized first and are subsequently modified with polyvinylpyrrolidone (PVP), PEG or other macromolecule materials to improve their biochemical stability; finally, they grow *in situ* or are dispersed in the framework of nano-MOFs.[139] The photosensitive materials can also be placed on the outer surfaces of nano-MOFs. This method generally uses the free metal ions on the outer surfaces of the nano-MOFs to coordinate with the photosensitive material to produce the outer wrapping of nano-MOFs. Fig. 17 shows the encapsulation of UiO-66 by ICG and Zr^{4+} outside UiO-66 for enhanced PDT, and finally the exterior is wrapped with red blood cell membrane (RBC) to increase its biocompatibility.[140]

5.3 Other

RT refers to the use of radioisotopes to produce α, β, γ and X-rays for cancer therapy, whose high penetration ability can kill cells in fixed points.[141] However, the low oxygen content and poor blood flow of cells can directly decrease their sensitivity.[142] In fact, tumor tissue generally grows tightly, thus resulting in poor blood flow and low oxygen content in tumor cells, and inevitably causing obstacles in the application of tumor RT. The most common method for treating tumors with nanomaterials is increasing the oxygen content of tumor cells or introducing radiosensitizers with an X-ray attenuation coefficient, thereby improving the RT effect. Carbonic anhydrase is overexpressed in tumors and is associated with the decrease in tumor oxygen content.[143,144] For example, Zr-MOF binds the Zn^{2+} of carbonic anhydrase in tumor cells, thus deactivating carbonic anhydrase IX (CA IX) and increasing the oxygen content in tumors.[145] Finally, the RT sensitizer quercetin loaded in Zr-MOF participates in the RT process and significantly enhances the

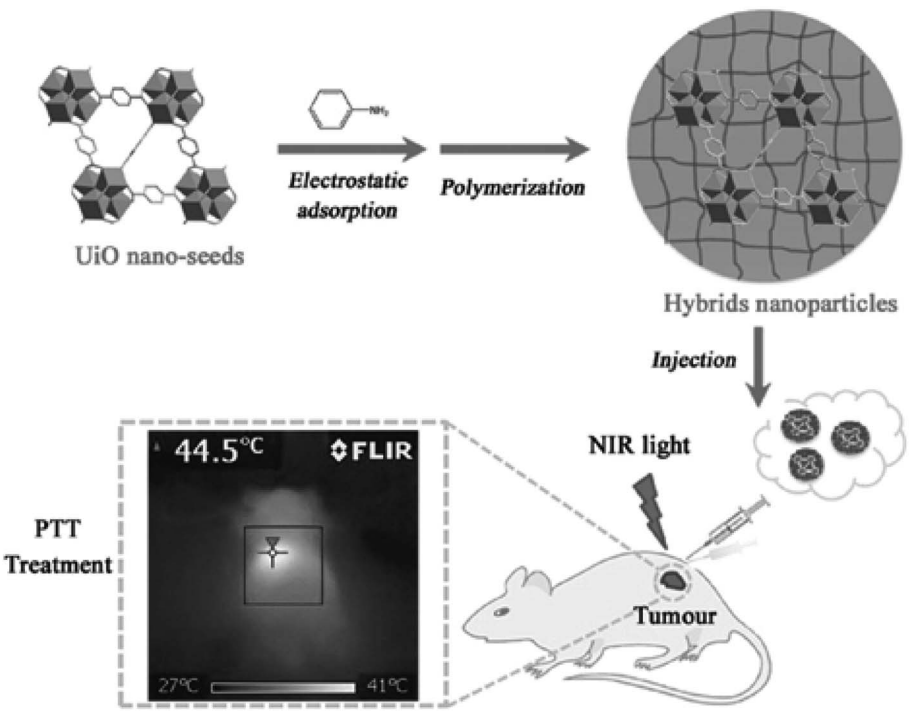

Fig. 15 Schematic presentation of UiO-66 hybrids and their application in PTT.[15] This figure has been adapted from ref. 15 with permission from Wiley-VCH Verlag & Co. KGaA, copyright 2016.

therapeutic effect (Fig. 18). In addition, the oxygen content in tumors can be increased with Mn^{3+} porphyrin or nano-MOFs with catalytic activity, thus achieving RT effects by integrating metal ions that effectively absorb X-rays.[94,146]

Imaging-guided therapy can precisely reveal tumor location and shape, thus leading to wide biomedical applications,[147] particularly in the treatment of cancers. These applications include MRI, computed tomography (CT) and fluorescence imaging.[148,149] MRI, a routine clinical examination method, does not involve radiation, and it produces three-dimensional imaging at high resolution; therefore, it is important in the evaluation of tumor detection, chemotherapy or other methods of treatment. The metal ions Gd^{3+} and Fe^{3+}, with paramagnetic or superparamagnetic properties, can alter the relaxation time of water protons in the surrounding medium under a magnetic field, thereby producing a good MRI effect. The introduction of these paramagnetic or superparamagnetic metal ions into the structure of the nano-MOFs can extend the applications of these materials. These metal ions can also be used to coordinate with a suitable organic chain to produce new nano-MOFs for imaging. Through scanning a certain thickness of a tissue with X-rays, images of different gradations can be formed *via* CT imaging according to the difference in absorption coefficients of X-rays between different tissue components. For example, H. Zhang *et al.* have synthesized ZIF-8 with incorporated Janus nanoparticles (gold modified by polyacrylic acid)[150] and reported their good CT imaging capability (Fig. 19). For fluorescence imaging, photons and molecules are used to generate electrons and cause their transition from the ground state to the excited state and back to the ground state, thus releasing energy in the form of fluorescence. Lanthanide metal ions have special optical properties in NIR. Y. Li *et al.* have synthesized rare earth miscellaneous $NaYF_4$:Yb, Er upconversion nanoparticles (UCNPs) with a particle size of approximately 40 nm, modified PVP and coated with a Fe-MIL-101_NH_2 shell.[151] *In vivo* experiments have indicated the good fluorescence imaging ability of this material, thus enabling fluorescence induction therapy (Fig. 20).

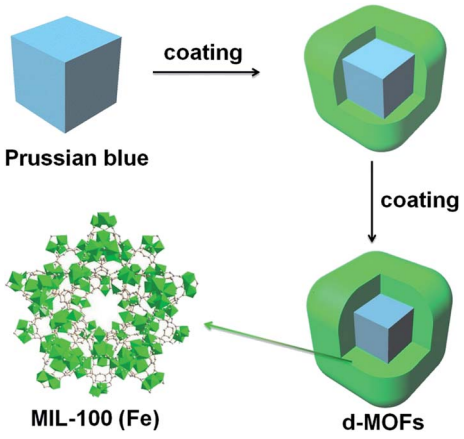

Fig. 16 Synthesis and characterization of the core–shell d-MOFs.[34] This figure has been reproduced from ref. 34 with permission from Elsevier, copyright 2016.

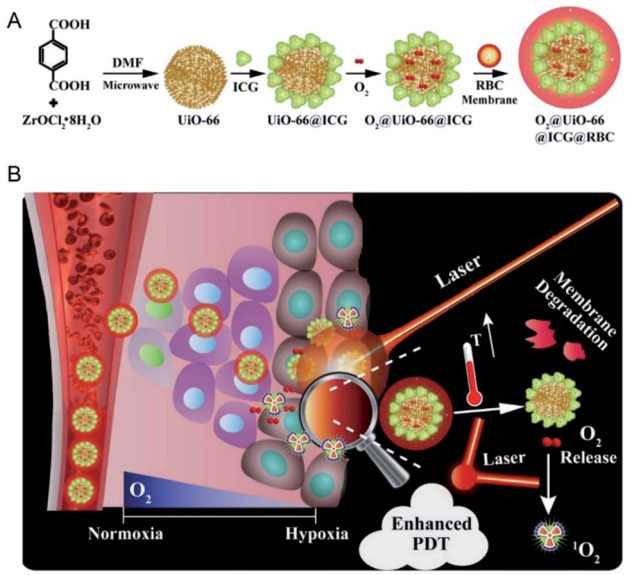

Fig. 17 Schemes of (A) the preparation of O_2@UiO-66@ICG@RBC and (B) the NIR-triggered O_2 releasing and enhanced PDT mechanism.[140] This figure has been adapted from ref. 140 with permission from Elsevier, copyright 2018.

Cooperative treatment is a broad concern in human disease treatment, because the therapeutic effects of synergistic treatment can often exceed those of single treatments. In recent tumor treatments, increasing attention has been paid to combined therapy with nano-MOFs. For better understanding of the research progress in this area, we summarize the treatment methods associated with nano-MOFs applied in combined therapy in recent years in Table 3.

6. Conclusions and prospects

Recent advances in cancer treatment based on nano-MOFs have been summarized, and the roles of nano-MOFs have

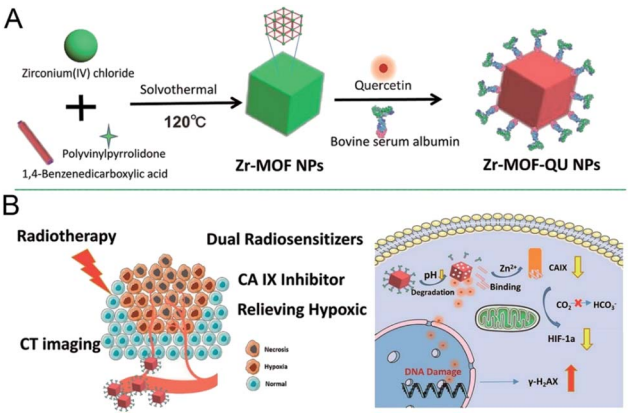

Fig. 18 Scheme of (A) synthesizing the Zr-MOF-QU (QU = quercetin) nanocomposites and (B) the NPs based dual sensitization radiation therapy of tumors and the mechanism of relieving hypoxia in the tumor microenvironment.[145] This figure has been adapted from ref. 145 with permission from American Chemical Society, copyright 2019.

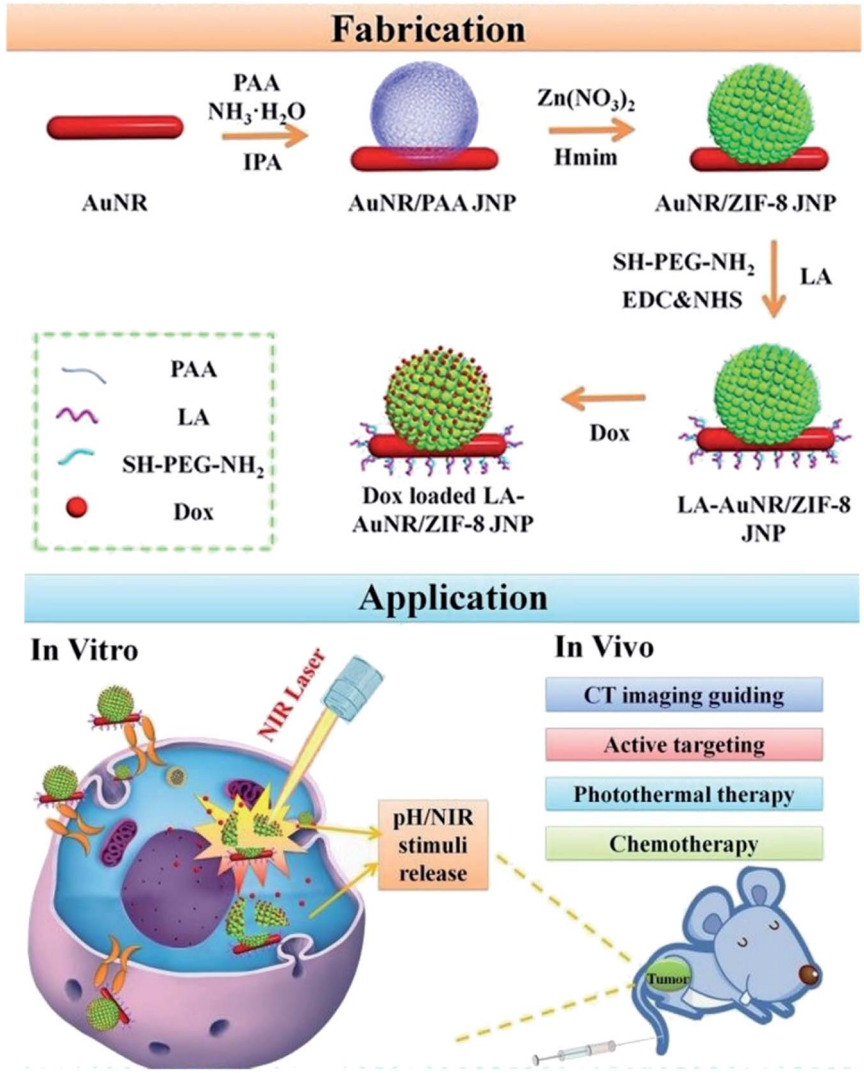

Fig. 19 Scheme of fabricating the lactobionic acid (LA)-AuNR/ZIF-8 NPs for dual NIR/pH triggered, CT imaging guided and targeted synergistic chemotherapy and photothermal therapy of liver cancer *in vitro* and *in vivo*.[150] This figure has been adapted from ref. 150 with permission from Royal Society of Chemistry, copyright 2013.

been described in detail. As drug carriers, the unique framework structure of nano-MOFs makes it possible to have a high drug loading, to be easily modified, to improve the biocompatibility through further modification, and to facilitate the responsive drug release. However, currently there are still some obstacles for nano-MOFs as drug carriers. Besides

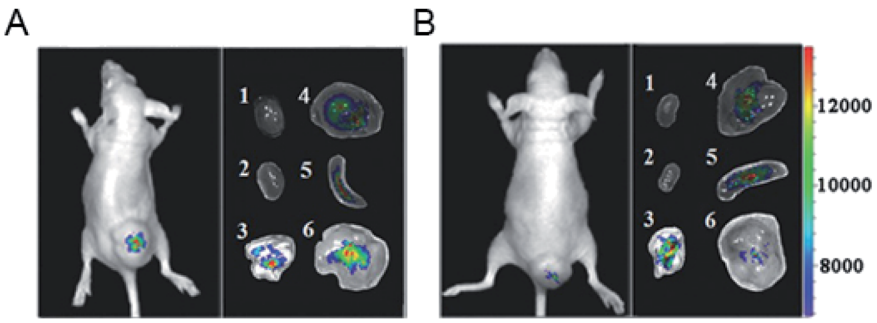

Fig. 20 Representative upconversion luminescence (UCL) imaging of subcutaneous KB tumor-bearing mice (tumor diameter: 8–10 mm) and dissected organs of the mice sacrificed 24 h after intravenous injection of (A) PEGylated core–shell UCNP@Fe-MIL-101_NH_2 @PEG-FA (target, FA = folic acid) and (B) UCNP@Fe-MIL-101_NH_2 (control). (1) Heart; (2) kidney; (3) lung; (4) liver; (5) spleen; (6) KB tumor. All images were acquired at a power density of 100 mW cm^{-2} on the skin.[151] This figure has been reproduced from ref. 151 with permission from Wiley-VCH Verlag & Co. KGaA, copyright 2015.

Table 3 Examples of MOF nanomaterials as a combined therapy

Combination type	MOFs	Functional components	Ref.
Luminescence-monitored drug delivery/PDT	UiO-66-NH_2@$NaYF_4$:Yb/Er	$NaYF_4$:Yb/Er	152
Chemotherapy/PTT	CuS@ZIF-8	CuS, quercetin	130
	MIL-100	Curcumin	124
	MIL-53 (Fe)	DOX, PPy	14
	ZIF-8	Cytarabine	153
Chemotherapy/PDT	NH_2-MIL-125	DOX	154
	CPC@MOF	Camptothecine, Ce6	155
	ZIF-8	DOX, g-C_3N_4	156
	Zr(IV)-based porphyrinic	α-Cyano-4-hydroxycinnamate, porphyrinic	157
Immunotherapy/PDT	TBP-MOF	TBP	158
PTT/PDT	Fe-soc-MOF@PEG-NH_2-ICG	ICG	159
	Hf-UiO-66	TCPC, porphyrin	160
	Cu-TCPP	Cu, TCPP	161
	Hf-UiO-66	Hf, TAPC	162
	Zr–FeP, siRNA	Porphyrin	113

certain toxic and side effects of the nano-MOFs, the low biodegradability of the drug carriers and the limited clinical application need to be significantly improved in the future. The development of a more versatile, safe and efficient drug delivery system on the basis of traditional responsive drug release is a promising research direction. Although some progress in tumor treatment has been made by using MOF-based biomaterials, some shortcomings continue to limit their application, such as the toxicity of metal ions inside nano-MOFs, and the trapping of nano-MOFs in the liver and spleen, thereby decreasing the therapeutic effects. Therefore, the following points are proposed: (1) the early biological application of nano-MOFs has mainly relied on its porosity and high specific surface area, which can adsorb drugs for chemotherapy with better therapeutic effects in synergistic treatments. However, much room for exploration remains. (2) The structural mechanisms of the existing synthetic nano-MOFs are unclear and require substantial further exploration. (3) Although research on the anti-tumor applications of nano-MOFs has undergone many years of development, the amounts and types of MOF-based nanomaterials applied to the human body remain limited; therefore, further efforts are needed to expand the range of nano-MOFs for biological applications.

Conflicts of interest

The authors declare no conflict of interest.

Acknowledgements

This work was financially supported by the Natural Science Foundation of Shanghai (19ZR1434800, 19ZR1461900).

References

1 Z. Hu, B. J. Deibert and J. Li, *Chem. Soc. Rev.*, 2014, **43**, 5815–5840.
2 J.-R. Li, R. J. Kuppler and H.-C. Zhou, *Chem. Soc. Rev.*, 2009, **38**, 1477–1504.
3 M. Hirscher and B. Panella, *Scr. Mater.*, 2007, **56**, 809–812.
4 Y.-S. Kang, Y. Lu, K. Chen, Y. Zhao, P. Wang and W.-Y. Sun, *Coord. Chem. Rev.*, 2019, **378**, 262–280.
5 M.-X. Wu and Y.-W. Yang, *Adv. Mater.*, 2017, **29**, 1606134.
6 S. Ahmed and C. Eng, *Curr. Oncol. Rep.*, 2018, **20**, 3.
7 T. M. Allen and P. R. Cullis, *Adv. Drug Delivery Rev.*, 2013, **65**, 36–48.
8 Y. Bae, N. Nishiyama, S. Fukushima, H. Koyama, M. Yasuhiro and K. Kataoka, *Bioconjugate Chem.*, 2005, **16**, 122–130.
9 S. Kumar, S. Jain, M. Nehra, N. Dilbaghi, G. Marrazza and K.-H. Kim, *Coord. Chem. Rev.*, 2020, **420**, 213407.
10 H. Deng, F. Dai, G. Ma and X. Zhang, *Adv. Mater.*, 2015, **27**, 3645–3653.
11 M. Lismont, L. Dreesen and S. Wuttke, *Adv. Funct. Mater.*, 2017, **27**, 1606314.
12 J. Della Rocca, D. Liu and W. Lin, *Acc. Chem. Res.*, 2011, **44**, 957–968.
13 W. Cai, J. Wang, C. Chu, W. Chen, C. Wu and G. Liu, *Adv. Sci.*, 2019, **6**, 1801526.
14 J. Huang, N. Li, C. Zhang and Z. Meng, *ACS Appl. Mater. Interfaces*, 2018, **10**, 38729–38738.
15 W. Wang, L. Wang, Y. Li, S. Liu, Z. Xie and X. Jing, *Adv. Mater.*, 2016, **28**, 9320–9325.
16 Z.-Q. Li, L.-G. Qiu, T. Xu, Y. Wu, W. Wang, Z.-Y. Wu and X. Jiang, *Mater. Lett.*, 2009, **63**, 78–80.
17 W. J. Son, J. Kim, J. Kim and W. S. Ahn, *Chem. Commun.*, 2008, 6336–6338.
18 T. Chalati, P. Horcajada, R. Gref, P. Couvreur and C. Serre, *J. Mater. Chem.*, 2011, **21**, 2220–2227.
19 X. Wu, Z. Bao, B. Yuan, J. Wang, Y. Sun, H. Luo and S. Deng, *Microporous Mesoporous Mater.*, 2013, **180**, 114–122.
20 W. Liang and D. M. D'Alessandro, *Chem. Commun.*, 2013, **49**, 3706–3708.
21 Z. Wang, Z. Li, M. Ng and P. J. Milner, *Dalton Trans.*, 2020, **49**, 16238–16244.

22 R. Zhang, C. A. Tao, R. Chen, L. Wu, X. Zou and J. Wang, *Nanomaterials*, 2018, **8**, 1067.
23 S. Khazalpour, V. Safarifard, A. Morsali and D. Nematollahi, *RSC Adv.*, 2015, **5**, 36547–36551.
24 Y. Liu, Y. Wei, M. Liu, Y. Bai, X. Wang, S. Shang, J. Chen and Y. Liu, *Angew. Chem., Int. Ed.*, 2020, **5**, 36547–36551.
25 A. Gao, X.-L. Hu, M. Saeed, B.-F. Chen, Y.-P. Li and H.-J. Yu, *Acta Pharmacol. Sin.*, 2019, **40**, 1129–1137.
26 J. B. Tagne, S. Kakumanu, D. Ortiz, T. Shea and R. J. Nicolosi, *Mol. Pharm.*, 2008, **5**, 280–286.
27 C. Wang, X. Wang, K. Dong, J. Luo, Q. Zhang and Y. Cheng, *Biomaterials*, 2016, **104**, 129–137.
28 Y. Yi, G. Lin, S. Chen, J. Liu, H. Zhang and P. Mi, *Mater. Sci. Eng., C*, 2018, **83**, 218–232.
29 A. Jin, Y. Wang, K. Lin and L. Jiang, *Bioact. Mater.*, 2020, **5**, 522–541.
30 C. Ding, L. Tong, J. Feng and J. Fu, *Molecules*, 2016, **21**, 1715.
31 W. Cai, C.-C. Chu, G. Liu and Y.-X. J. Wang, *Small*, 2015, **11**, 4806–4822.
32 H. Zheng, Y. Zhang, L. Liu, W. Wan, P. Guo, A. M. Nystrom and X. Zou, *J. Am. Chem. Soc.*, 2016, **138**, 962–968.
33 R. Abazari, A. R. Mahjoub, F. Ataei, A. Morsali, C. L. Carpenter-Warren, K. Mehdizadeh and A. M. Z. Slawin, *Inorg. Chem.*, 2018, **57**, 13364–13379.
34 D. Wang, J. Zhou, R. Chen, R. Shi, G. Zhao, G. Xia, R. Li, Z. Liu, J. Tian, H. Wang, Z. Guo, H. Wang and Q. Chen, *Biomaterials*, 2016, **100**, 27–40.
35 K. Jiang, L. Zhang, Q. Hu, Y. Yang, W. Lin, Y. Cui, Y. Yang and G. Qian, *Mater. Lett.*, 2018, **225**, 142–144.
36 X. Leng, X. Dong, W. Wang, N. Sai, C. Yang, L. You, H. Huang, X. Yin and J. Ni, *Molecules*, 2018, **23**, 2490.
37 A. Cabrera-Garcia, E. Checa-Chavarria, E. Rivero-Buceta, V. Moreno, E. Fernandez and P. Botella, *J. Colloid Interface Sci.*, 2019, **541**, 163–174.
38 X.-G. Wang, Z.-Y. Dong, H. Cheng, S.-S. Wan, W.-H. Chen, M.-Z. Zou, J.-W. Huo, H.-X. Deng and X.-Z. Zhang, *Nanoscale*, 2015, **7**, 16061–16070.
39 Q. Hu, J. Yu, M. Liu, A. Liu, Z. Dou and Y. Yang, *J. Med. Chem.*, 2014, **57**, 5679–5685.
40 J. An, S. J. Geib and N. L. Rosi, *J. Am. Chem. Soc.*, 2009, **131**, 8376–8377.
41 L.-L. Tan, H. Li, Y. Zhou, Y. Zhang, X. Feng, B. Wang and Y.-W. Yang, *Small*, 2015, **11**, 3807–3813.
42 W.-H. Chen, X. Yu, A. Cecconello, Y. S. Sohn, R. Nechushtai and I. Willner, *Chem. Sci.*, 2017, **8**, 5769–5780.
43 J. S. Kahn, L. Freage, N. Enkin, M. A. A. Garcia and I. Willner, *Adv. Mater.*, 2017, **29**, 1602782.
44 R. Cheng, F. Feng, F. Meng, C. Deng, J. Feijen and Z. Zhong, *J. Controlled Release*, 2011, **152**, 2–12.
45 Q. Xue, C. Ye, M. Zhang, X. Hu and T. Cai, *J. Colloid Interface Sci.*, 2019, **551**, 39–46.
46 J. Zhao, Y. Yang, X. Han, C. Liang, J. Liu, X. Song, Z. Ge and Z. Liu, *ACS Appl. Mater. Interfaces*, 2017, **9**, 23555–23563.
47 B. Lei, M. Wang, Z. Jiang, W. Qi, R. Su and Z. He, *ACS Appl. Mater. Interfaces*, 2018, **10**, 16698–16706.
48 Y. Duan, F. Ye, Y. Huang, Y. Qin, C. He and S. Zhao, *Chem. Commun.*, 2018, **54**, 5377–5380.
49 W. Lin, Q. Hu, J. Yu, K. Jiang, Y. Yang, S. Xiang, Y. Cui, Y. Yang, Z. Wang and G. Qian, *ChemPlusChem*, 2016, **81**, 804–810.
50 W. Lin, Q. Hu, K. Jiang, Y. Cui, Y. Yang and G. Qian, *Microporous Mesoporous Mater.*, 2017, **249**, 55–60.
51 F. Ke, Y.-P. Yuan, L.-G. Qiu, Y.-H. Shen, A.-J. Xie, J.-F. Zhu, X.-Y. Tian and L.-D. Zhang, *J. Mater. Chem.*, 2011, **21**, 3843–3848.
52 Y.-n. Wu, M. Zhou, S. Li, Z. Li, J. Li, A. Wu, G. Li, F. Li and X. Guan, *Small*, 2014, **10**, 2927–2936.
53 S. Sharma, K. Sethi and I. Roy, *New J. Chem.*, 2017, **41**, 11860–11866.
54 J. Fang, Y. Yang, W. Xiao, B. Zheng, Y. B. Lv, X. L. Liu and J. Ding, *Nanoscale*, 2016, **8**, 3259–3263.
55 K. Jiang, L. Zhang, Q. Hu, D. Zhao, T. Xia, W. Lin, Y. Yang, Y. Cui, Y. Yang and G. Qian, *J. Mater. Chem. B*, 2016, **4**, 6398–6401.
56 M. H. Teplerisky, M. Fantham, P. Li, T. C. Wang, J. P. Mehta, L. J. Young, P. Z. Moghadam, J. T. Hupp, O. K. Farha, C. F. Kaminski and D. Fairen-Jimenez, *J. Am. Chem. Soc.*, 2017, **139**, 7522–7532.
57 W. Morris, W. E. Briley, E. Auyeung, M. D. Cabezas and C. A. Mirkin, *J. Am. Chem. Soc.*, 2014, **136**, 7261–7264.
58 W.-H. Chen, X. Yu, W.-C. Liao, Y. S. Sohn, A. Cecconello, A. Kozell, R. Nechushtai and I. Willner, *Adv. Funct. Mater.*, 2017, **27**, 1702102.
59 W.-H. Chen, W.-C. Liao, Y. S. Sohn, M. Fadeev, A. Cecconello, R. Nechushtai and I. Willner, *Adv. Funct. Mater.*, 2018, **28**, 1705137.
60 Y. Zhang, H. Fu, S. Chen, B. Liu, W. Sun and H. Gao, *Chem. Commun.*, 2020, **56**, 762–765.
61 S. Nagata, K. Kokado and K. Sada, *CrystEngComm*, 2020, **22**, 1106–1111.
62 Y. Liu, C. S. Gong, Y. Dai, Z. Yang, G. Yu, Y. Liu, M. Zhang, L. Lin, W. Tang, Z. Zhou, G. Zhu, J. Chen, O. Jacobson, D. O. Kiesewetter, Z. Wang and X. Chen, *Biomaterials*, 2019, **218**, 119365.
63 J. W. Brown, B. L. Henderson, M. D. Kiesz, A. C. Whalley, W. Morris, S. Grunder, H. Deng, H. Furukawa, J. I. Zink, J. F. Stoddart and O. M. Yaghi, *Chem. Sci.*, 2013, **4**, 2858–2864.
64 X. Meng, B. Gui and D. Yuan, *Sci. Adv.*, 2016, **2**, e1600480.
65 Z. Luo, L. Jiang, S. Yang, Z. Li, W. M. W. Soh, L. Zheng, X. J. Loh and Y. L. Wu, *Adv. Healthcare Mater.*, 2019, **8**, e1900406.
66 M.-X. Wu, J. Gao, F. Wang, J. Yang, N. Song, X. Jin, P. Mi, J. Tian, J. Luo, F. Liang and Y.-W. Yang, *Small*, 2018, **14**, 1704440.
67 L.-L. Tan, N. Song, S. X.-A. Zhang, H. Li, B. Wang and Y.-W. Yang, *J. Mater. Chem. B*, 2016, **4**, 135–140.
68 S. Y. Tan, C. Y. Ang, A. Mahmood, Q. Qu, P. Li, R. Zou and Y. Zhao, *ChemNanoMat*, 2016, **2**, 504–508.
69 G. Cheng, W. Li, L. Ha, X. Han, S. Hao, Y. Wan, Z. Wang, F. Dong, X. Zou, Y. Mao and S.-Y. Zheng, *J. Am. Chem. Soc.*, 2018, **140**, 7282–7291.

70 H. Zhang, J. Zhang, Q. Li, A. Song, H. Tian, J. Wang, Z. Li and Y. Luan, *Biomaterials*, 2020, **245**, 119983.
71 Y. Cai, Z. Sheng and J. Wang, *Z. Anorg. Allg. Chem.*, 2018, **644**, 877–882.
72 A. R. Chowdhuri, T. Singh, S. K. Ghosh and S. K. Sahu, *ACS Appl. Mater. Interfaces*, 2016, **8**, 16573–16583.
73 T. A. Vahed, M. R. Naimi-Jamal and L. Panahi, *New J. Chem.*, 2018, **42**, 11137–11146.
74 Y. Yang, F. Xia, Y. Yang, B. Gong, A. Xie, Y. Shen and M. Zhu, *J. Mater. Chem. B*, 2017, **5**, 8600–8606.
75 Z. C. Wang, Y. Zhang and Z. Y. Li, *J. Cluster Sci.*, 2018, **29**, 1285–1290.
76 X. Du, R. Fan, L. Qiang, K. Xing, H. Ye, X. Ran, Y. Song, P. Wang and Y. Yang, *ACS Appl. Mater. Interfaces*, 2017, **9**, 28939–28948.
77 Y. Miao, X. Zhao, Y. Qiu, Z. Liu, W. Yang and X. Jia, *ACS Appl. Bio Mater.*, 2019, **2**, 895–905.
78 K. Jiang, L. Zhang, Q. Hu, Q. Zhang, W. Lin, Y. Cui, Y. Yang and G. Qian, *Chem.–Eur. J.*, 2017, **23**, 10215–10221.
79 Y. Kim, R. Haldar, H. Kim, J. Koo and K. Kim, *Dalton Trans.*, 2016, **45**, 4187–4192.
80 C. Huang, W. Tan, J. Zheng, C. Zhu, J. Huo and R. Yang, *ACS Appl. Mater. Interfaces*, 2019, **11**, 25740–25749.
81 W.-H. Chen, G.-F. Luo, Y. S. Sohn, R. Nechushtai and I. Willner, *Adv. Funct. Mater.*, 2019, **29**, 1805341.
82 G. Zhou, Y. S. Wang, Z. Jin, P. Zhao, H. Zhang, Y. Wen and Q. He, *Nanoscale Horiz.*, 2019, **4**, 1185–1193.
83 X. Gao, R. Cui, M. Zhang and Z. Liu, *Mater. Lett.*, 2017, **197**, 217–220.
84 K. Dong, Z. Wang, Y. Zhang, J. Ren and X. Qu, *ACS Appl. Mater. Interfaces*, 2018, **10**, 31998–32005.
85 Y.-D. Zhu, S.-P. Chen, H. Zhao, Y. Yang, X.-Q. Chen, J. Sun, H.-S. Fan and X.-D. Zhang, *ACS Appl. Mater. Interfaces*, 2016, **8**, 34209–34217.
86 Y. Li, J. Jin, D. Wang, J. Lv, K. Hou, Y. Liu, C. Chen and Z. Tang, *Nano Res.*, 2018, **11**, 3294–3305.
87 W. Zhou, L. Wang, F. Li, W. Zhang, W. Huang, F. Huo and H. Xu, *Adv. Funct. Mater.*, 2017, **27**, 1605465.
88 W.-H. Chen, G.-F. Luo, M. Vazquez-Gonzalez, R. Cazelles, Y. S. Sohn, R. Nechushtai, Y. Mandel and I. Willner, *ACS Nano*, 2018, **12**, 7538–7545.
89 Y. Chen, P. Li, J. A. Modica, R. J. Drout and O. K. Farha, *J. Am. Chem. Soc.*, 2018, **140**, 5678–5681.
90 M. A. Luzuriaga, R. P. Welch, M. Dharmarwardana, C. E. Benjamin, S. B. Li, A. Shahrivarkevishahi, S. Popal, L. H. Tuong, C. T. Creswel and J. J. Gassensmith, *ACS Appl. Mater. Interfaces*, 2019, **11**(10), 9740–9746.
91 S. Shams, W. Ahmad, A. H. Memon, S. Shams, Y. Wei, Q. Yuan and H. Liang, *New J. Chem.*, 2020, **44**, 17671–17678.
92 L. Sun, Y. Xu, Y. Gao, X. Huang, S. Feng, J. Chen, X. Wang, L. Guo, M. Li, X. Meng, J. Zhang, J. Ge, X. An, D. Ding, Y. Luo, Y. Zhang, Q. Jiang and X. Ning, *Small*, 2019, **15**, 1901156.
93 X. Gao, G. Ji, R. Cui and Z. Liu, *Mater. Lett.*, 2019, **237**, 197–199.
94 Z. He, X. Huang, C. Wang, X. Li, Y. Liu, Z. Zhou, S. Wang, F. Zhang, Z. Wang, O. Jacobson, J.-J. Zhu, G. Yu, Y. Dai and X. Chen, *Angew. Chem., Int. Ed.*, 2019, **58**, 8752–8756.
95 F. Wang, Y. Zhang, Z. Liu, Z. Du, L. Zhang, J. Ren and X. Qu, *Angew. Chem., Int. Ed.*, 2019, **58**, 6987–6992.
96 G. Lan, K. Ni, Z. Xu, S. S. Veroneau, Y. Song and W. Lin, *J. Am. Chem. Soc.*, 2018, **140**, 5670–5673.
97 J. Park, Q. Jiang, D. Feng, L. Mao and H.-C. Zhou, *J. Am. Chem. Soc.*, 2016, **138**, 3518–3525.
98 H. Zhang, X.-T. Tian, Y. Shang, Y.-H. Li and X.-B. Yin, *ACS Appl. Mater. Interfaces*, 2018, **10**, 28390–28398.
99 H. Min, J. Wang, Y. Qi, Y. Zhang, X. Han, Y. Xu, J. Xu, Y. Li, L. Chen, K. Cheng, G. Liu, N. Yang, Y. Li and G. Nie, *Adv. Mater.*, 2019, **31**, 1808200.
100 S.-S. Wan, Q. Cheng, X. Zeng and X.-Z. Zhang, *ACS Nano*, 2019, **13**, 6561–6571.
101 K. Bhattacharya, S. P. Mukherjee, A. Gallud, S. C. Burkert, S. Bistarelli, S. Bellucci, M. Bottini, A. Star and B. Fadeel, *Nanomed. Nanotechnol. Biol. Med.*, 2016, **12**, 333–351.
102 P. Yang, Y. Tian, Y. Men, R. Guo, H. Peng, Q. Jiang and W. Yang, *ACS Appl. Mater. Interfaces*, 2018, **10**, 42039–42049.
103 X. Pan, L. Bai, H. Wang, Q. Wu, H. Wang, S. Liu, B. Xu, X. Shi and H. Liu, *Adv. Mater.*, 2018, **30**, e1800180.
104 J. Qi, W. Li, K. Lu, F. Jin, D. Liu, X. Xu, X. Wang, X. Kang, W. Wang, G. Shu, F. Han, X. Ying, J. You, J. Ji and Y. Du, *Nano Lett.*, 2019, **19**, 4949–4959.
105 J. Xu, X. Cheng, L. Tan, C. Fu, M. Ahmed, J. Tian, J. Dou, Q. Zhou, X. Ren, Q. Wu, S. Tang, H. Zhou, X. Meng, J. Yu and P. Liang, *Nano Lett.*, 2019, **19**, 2914–2927.
106 Q. Wu, N. Xia, D. Long, L. Tan, W. Rao, J. Yu, C. Fu, X. Ren, H. Li, L. Gou, P. Liang, J. Ren, L. Li and X. Meng, *Nano Lett.*, 2019, **19**, 5277–5286.
107 C. Fu, H. Zhou, L. Tan, Z. Huang, Q. Wu, X. Ren, J. Ren and X. Meng, *ACS Nano*, 2018, **12**, 2201–2210.
108 T. Li, Q. Wu, W. Wang, Z. Chen, L. Tan, J. Yu, C. Fu, X. Ren, P. Liang, J. Ren, L. Ma and X. Meng, *Biomaterials*, 2020, **234**, 119773.
109 Z. Deng, C. Fang, X. Ma, X. Li, Y. J. Zeng and X. Peng, *ACS Appl. Mater. Interfaces*, 2020, **12**, 20321–20330.
110 T. Xue, C. Xu, Y. Wang, Y. Wang, H. Tian and Y. Zhang, *Biomater. Sci.*, 2019, **7**, 4615–4623.
111 J. Liu, Y. Yang, W. Zhu, X. Yi, Z. Dong, X. Xu, M. Chen, K. Yang, G. Lu, L. Jiang and Z. Liu, *Biomaterials*, 2016, **97**, 1–9.
112 W. Zhang, J. Lu, X. Gao, P. Li, W. Zhang, Y. Ma, H. Wang and B. Tang, *Angew. Chem., Int. Ed.*, 2018, **57**, 4891–4896.
113 K. Zhang, X. Meng, Y. Cao, Z. Yang, H. Dong, Y. Zhang, H. Lu, Z. Shi and X. Zhang, *Adv. Funct. Mater.*, 2018, **28**, 1804634.
114 Q. L. Li, Y. Sun, L. Ren, X. Wang, C. Wang, L. Li, Y. W. Yang, X. Yu and J. Yu, *ACS Appl. Mater. Interfaces*, 2018, **10**, 29314–29324.
115 Z. Xiao, C. Xu, X. Jiang, W. Zhang, Y. Peng, R. Zou, X. Huang, Q. Liu, Z. Qin and J. Hu, *Nano Res.*, 2016, **9**, 1934–1947.

116 X. Cheng, R. Sun, L. Yin, Z. Chai, H. Shi and M. Gao, *Adv. Mater.*, 2017, **29**, 1604894.
117 L. Zou, H. Wang, B. He, L. Zeng, T. Tan, H. Cao, X. He, Z. Zhang, S. Guo and Y. Li, *Theranostics*, 2016, **6**, 762–772.
118 Y. H. Xu, Y. L. Shan, H. L. Cong, Y. Q. Shen and B. Yu, *Curr. Pharm. Des.*, 2018, **24**, 4060–4076.
119 J. Chen, C. Ning, Z. Zhou, P. Yu, Y. Zhu, G. Tan and C. Mao, *Prog. Mater. Sci.*, 2019, **99**, 1–26.
120 X. Song, C. Liang, H. Gong, Q. Chen, C. Wang and Z. Liu, *Small*, 2015, **11**, 3932–3941.
121 T. T. V. Phan, S. Bharathiraja, V. T. Nguyen, M. S. Moorthy, P. Manivasagan, K. D. Lee and J. Oh, *RSC Adv.*, 2017, **7**, 35027–35037.
122 S. Wang, Z. Zhou, G. Yu, N. Lu, Y. Liu, Y. Dai, X. Fu, J. Wang and X. Chen, *ACS Appl. Mater. Interfaces*, 2018, **10**, 28382–28389.
123 X. Cai, X. Deng, Z. Xie, Y. Shi, M. Pang and J. Lin, *Chem. Eng. J.*, 2019, **358**, 369–378.
124 Y. Zhang, L. Wang, L. Liu, L. Lin, F. Liu, Z. Xie, H. Tian and X. Chen, *ACS Appl. Mater. Interfaces*, 2018, **10**, 41035–41045.
125 J. Feng, Z. Xu, P. Dong, W. Yu, F. Liu, Q. Jiang, F. Wang and X. Liu, *J. Mater. Chem. B*, 2019, **7**, 994–1004.
126 Z. Li, Y. Hu, Z. Miao, H. Xu, C. Li, Y. Zhao, Z. Li, M. Chang, Z. Ma, Y. Sun, F. Besenbacher, P. Huang and M. Yu, *Nano Lett.*, 2018, **18**, 6778–6788.
127 X. Song, Q. Chen and Z. Liu, *Nano Res.*, 2015, **8**, 340–354.
128 M. Khafaji, M. Zamani, M. Golizadeh and O. Bavi, *Biophys. Rev.*, 2019, **11**, 335–352.
129 Z. Wang, X. Tang, X. Wang, D. Yang, C. Yang, Y. Lou, J. Chen and N. He, *Chem. Commun.*, 2016, **52**, 12210–12213.
130 W. Jiang, H. Zhang, J. Wu, G. Zhai, Z. Li, Y. Luan and S. Garg, *ACS Appl. Mater. Interfaces*, 2018, **10**, 34513–34523.
131 L. Zhang, C. Liu, Y. Gao, Z. Li, J. Xing, W. Ren, L. Zhang, A. Li, G. Lu, A. Wu and L. Zeng, *Adv. Healthcare Mater.*, 2018, **7**, 1801144.
132 Y. Lu, L. Li, Z. Lin, M. Li, X. Hu, Y. Zhang, M. Peng, H. Xia and G. Han, *Adv. Healthcare Mater.*, 2018, **29**, 2982–2993.
133 M. Mohammadniaei, T. Lee, B. G. Bharate, J. Yoon, H. K. Choi, S.-j. Park, J. Kim, J. Kim and J.-W. Choi, *Small*, 2018, **14**, 1802934.
134 Z. Tian, X. Yao, K. Ma, X. Niu, J. Grothe, Q. Xu, L. Liu, S. Kaskel and Y. Zhu, *ACS Omega*, 2017, **2**, 1249–1258.
135 A. K. Parchur, Q. Li and A. Zhou, *Biomater. Sci.*, 2016, **4**, 1781–1791.
136 J. Shao, C. Ruan, H. Xie, Z. Li, H. Wang, P. K. Chu and X.-F. Yu, *Adv. Sci.*, 2018, **5**, 1700848.
137 W. Song, Y. Li, Y. Wang, D. Wang, D. He, W. Chen, W. Yin and W. Yang, *J. Biomed. Nanotechnol.*, 2017, **13**, 1115–1123.
138 P. Yang, Y. Men, Y. Tian, Y. Cao, L. Zhang, X. Yao and W. Yang, *ACS Appl. Mater. Interfaces*, 2019, **11**, 11209–11219.
139 Y. Wang, W. Wu, J. Liu, P. N. Manghnani, F. Hu, D. Ma, C. Teh, B. Wang and B. Liu, *ACS Nano*, 2019, **13**, 6879–6890.
140 S. Gao, P. Zheng, Z. Li, X. Feng, W. Yan, S. Chen, W. Guo, D. Liu, X. Yang, S. Wang, X.-J. Liang and J. Zhang, *Biomaterials*, 2018, **178**, 83–94.
141 H. Ikushima, *J. Med. Investig.*, 2010, **57**, 1–11.
142 G. S. Song, L. Cheng, Y. Chao, K. Yang and Z. Liu, *Adv. Mater.*, 2017, **29**, 1700996.
143 G. C. Barnett, C. M. L. West, A. M. Dunning, R. M. Elliott, C. E. Coles, P. D. P. Pharoah and N. G. Burnet, *Nat. Rev. Cancer*, 2009, **9**, 134–142.
144 W. Li, X. Guo, F. Kong, H. Zhang, L. Luo, Q. Li, C. Zhu, J. Yang, Y. Du and J. You, *J. Controlled Release*, 2017, **258**, 171–181.
145 T. Ma, Y. Liu, Q. Wu, L. Luo, Y. Cui, X. Wang, X. Chen, L. Tan and X. Meng, *ACS Nano*, 2019, **13**, 4209–4219.
146 Y. Chen, H. Zhong, J. Wang, X. Wan, Y. Li, W. Pan, N. Li and B. Tang, *Chem. Sci.*, 2019, **10**, 5773–5778.
147 Y. Huang, S. He, W. Cao, K. Cai and X.-J. Liang, *Nanoscale*, 2012, **4**, 6135–6149.
148 H.-S. Wang, *Coord. Chem. Rev.*, 2017, **349**, 139–155.
149 C. Tian, L. Zhu, F. Lin and S. G. Boyes, *ACS Appl. Mater. Interfaces*, 2015, **7**, 17765–17775.
150 H. Zhang, Q. Zhang, C. Liu and B. Han, *Biomater. Sci.*, 2019, **7**, 1696–1704.
151 Y. Li, J. Tang, L. He, Y. Liu, Y. Liu, C. Chen and Z. Tang, *Adv. Mater.*, 2015, **27**, 4075–4080.
152 Z. Yuan, L. Zhang, S. Li, W. Zhang, M. Lu, Y. Pan, X. Xie, L. Huang and W. Huang, *J. Am. Chem. Soc.*, 2018, **140**, 15507–15515.
153 H. Zhang, Q. Li, R. Liu, X. Zhang, Z. Li and Y. Luan, *Adv. Funct. Mater.*, 2018, **28**, 1802830.
154 A. Rengaraj, P. Puthiaraj, N.-S. Heo, H. Lee, S. K. Hwang, S. Kwon, W.-S. Ahn and Y.-S. Huh, *Colloids Surf., B*, 2017, **160**, 1–10.
155 J. Liu, L. Zhang, J. Lei, H. Shen and H. Ju, *ACS Appl. Mater. Interfaces*, 2017, **9**, 2150–2158.
156 R. Chen, J. Zhang, Y. Wang, X. Chen, J. A. Zapien and C.-S. Lee, *Nanoscale*, 2015, **7**, 17299–17305.
157 Z.-X. Chen, M.-D. Liu, M.-K. Zhang, S.-B. Wang, L. Xu, C.-X. Li, F. Gao, B.-R. Xie, Z.-L. Zhong and X.-Z. Zhang, *Adv. Funct. Mater.*, 2018, **28**, 1803498.
158 J.-Y. Zeng, M.-Z. Zou, M. Zhang, X.-S. Wang, X. Zeng, H. Cong and X.-Z. Zhang, *ACS Nano*, 2018, **12**, 4630–4640.
159 X. Cai, B. Liu, M. Pang and J. Lin, *Dalton Trans.*, 2018, **47**, 16329–16336.
160 X. Zheng, L. Wang, M. Liu, P. Lei, F. Liu and Z. Xie, *Chem. Mater.*, 2018, **30**, 6867–6876.
161 B. Li, X. Wang, L. Chen, Y. Zhou, W. Dang, J. Chang and C. Wu, *Theranostics*, 2018, **8**, 4086–4096.
162 X. Zheng, L. Wang, Y. Guan, Q. Pei, J. Jiang and Z. Xie, *Biomaterials*, 2020, **235**, 119792.